Micro-Photosynthetic Power Cell Modeling, Sensing, and Energy Harvesting

Tamanwè Payarou

A Thesis
In
The Department
Of
Electrical and Computer Engineering

Presented in Partial Fulfillment of the Requirements
For the Degree of Master of Applied Science at
Concordia University
Montreal, Quebec, Canada

March 2018

CONCORDIA UNIVERSITY
SCHOOL OF GRADUATE STUDIES

This is to certify that the thesis prepared

By: Tamanwè Payarou

Entitled:

Micro-Photosynthetic Power Cell Modeling, Sensing, and Energy Harvesting

and submitted in partial fulfillment of the requirements for the degree of

Master of Applied Science

Complies with the regulations of this University and meets the accepted standards with respect to originality and quality.

Signed by the final examining committee:

_____ Chair
Dr. R. Raut

_____ Examiner, External
Dr. M. Packirisamy To the Program

_____ Examiner
Dr. Z. Kabir

_____ Supervisor
Dr. P. Pillay

Approved by: _____
Dr. W. E. Lynch, Chair
Department of Electrical and Computer Engineering

_____20_____ _____
Dr. Amir Asif, Dean
Faculty of Engineering and Computer Science

Abstract

Micro-Photosynthetic Power Cell Modeling, Sensing, and Energy Harvesting

Tamanwè Payarou

Micro-photosynthetic cells (μ-PSC) are considered as self-sustaining sources of energy that can be used for powering mobile microelectromechanical systems (MEMS) and remotely located sensor networks. Their ability to generate power under both dark and illuminated conditions, self-restoring capabilities, environmental friendliness, compactness, and low operation and maintenance cost are some of the advantages. Newly developed μ-PSCs can produce a maximum power density of several hundreds of mW/m^2. This work presents a real-time sensing circuit, an updated electrochemical model of μ-PSCs, and an energy harvester designed for power investigations of μ-PSCs. The proposed current sensing circuit is designed to provide accurate and dynamic current readings from nanoamperes (nA) up to few milliamperes (mA). The developed electrochemical model of μ-PSCs is based on knowledge accumulated from different fields such as chemical, biological and electrical sciences and on practical results. The photosynthesis and respiration of algae cells, as well as the effects of the irradiance, the day and night cycle, the temperature, and the pH of the solution, are included in the model. From the electrochemical model developed, a circuit level representation is derived. The validated electrochemical model is used to determine the maximum power point operation of μ-PSCs under various operating conditions. This provides an insight into designing efficient energy harvesters for μ-PSCs. An energy harvesting circuit is designed prototyped and tested. This work, therefore shifted the μ-PSC technology into practical field enabling μ-PSCs emulation and practical use of μ-PSCs in real applications.

Acknowledgment

Glory be to God who facilitated and made successful everything in this process. I would like to thank wholeheartedly Dr. Pragasen Pillay for the opportunity he provided me to be one of his students. This work would not have been possible without his professionalism, patience, valuable guidance and financial support.

I am grateful to my colleagues in Power Electronics and Energy Research (PEER) Group, Optical Bio-MEMS Laboratory at the Department of Mechanical and Industrial Engineering, and to all those with whom I had the pleasure to work during my study.

I would like to dedicate this work to my parents and family members for all their support, love and encouragement throughout my education process.

Table of Contents

List of Figures

List of Tables

Chapter 1: Introduction

1.1 Overview of micro photosynthetic power cells

Micro-photosynthetic cells are a green source of energy. They are able to produce power in dark and illuminated conditions. They are self-sustaining and self-restoring sources and can be used in different applications such as for mobile MEMS devices and remotely located sensor networks. In the search for innovative and environmentally friendly technologies, μ-PSCs presents themselves as important candidates with their compactness, and their low operation and maintenance cost [1]. Many factors such as irradiation, the day and night cycles, the pH, the temperature in the reaction chamber, and the nutrients are indispensable in the power generation process from μ-PSCs.

1.2 Principles of operation

1.2.1 Power generation concept

Micro photosynthetic power cells operate basically as hydrogen fuel cells. The protons diffuse through the proton-transfer membrane while the electrons follow the path provided through an external load. However, the source of fuel is different. The source of electricity in μ-PSCs comes from the interactions between the unicellular cells (algae) and their medium. *Fig. 1.1* shows the basic operation of μ-PSCs. The process starts in the anode chamber where a mix of algae and anolyte (solution in the anode chamber) is found and ends in the cathode chamber via proton exchange membrane and through the external path.

The anode is filled with a solution that ensures algae growth and sustainability. The anolyte acts as a mediator for the electrons diffusion into and out of the algae and siphons to liberate electrons. The texture of the anolyte may vary depending on the type of

microorganism present in the solution. Most the used anolytes are a good mix of nutrients such as carbon dioxide (CO_2), oxygen (O_2), nitrate ${NO_3}^-$, phosphate (${PO_4}^{3-}$). Methylene blue is used as mediator in most cases. The temperature and the pH of the anolyte are also important factors that are controlled for optimal growth of algae. The anode is made from a transparent material ensuring the photosynthesis process during the day cycle which can be represented by the equation in *(1. 1)*.

$$6CO_2 + 6H_2O \quad ==> \quad C_6H_{12}O_6 + 6O_2 \tag{1. 1}$$

During the photosynthesis process the electrons and protons are separated with the action of the mediator described in equations *(1. 2)* and *(1. 3)*, and found in [2] and [3]-[5].

$$Med + NADPH \ ==> \ Med_{red} + NADP^+ \tag{1. 2}$$

$$Med_{red} \ ==> 2e^- + H^+ + Med \tag{1. 3}$$

$NADP^+$ is the nicotinamide adenine dinucleotide phosphate.

$NADPH$ operates as a reducing agent or coenzyme for the reaction.

Med is the mediator and Med_{red} is the reduced mediator.

During the night cycle, respiration takes place. Generated glucose during the day cycle is used to produce electricity as described in equations *(1. 4)-(1. 6)* developed in [2] and [3]-[5].

$$C_6H_{12}O_6 + 6O_2 \quad ==> \quad 6CO_2 + 6H_2O \tag{1. 4}$$

$$Med + NADH \ ==> \ Med_{red} + NAD^+ \tag{1. 5}$$

$$Med_{red} \ ==> \ 2e^- + H^+ + Med \tag{1. 6}$$

NAD^+ is the nicotinamide adenine dinucleotide.

$NADH$ is the nicotinamide adenine dinucleotide dehydrogenase. It operate as a reducing agent or coenzyme for the reaction. The generation of the biological adenosine triphosphate is the result of multiple oxidation-reduction reactions including $NADH$.

The protons H^+ diffuses through the membrane to the cathode. The electrons liberated on the anode surface made with highly conducting materials will follow the external path through the load to reach the cathode chamber.

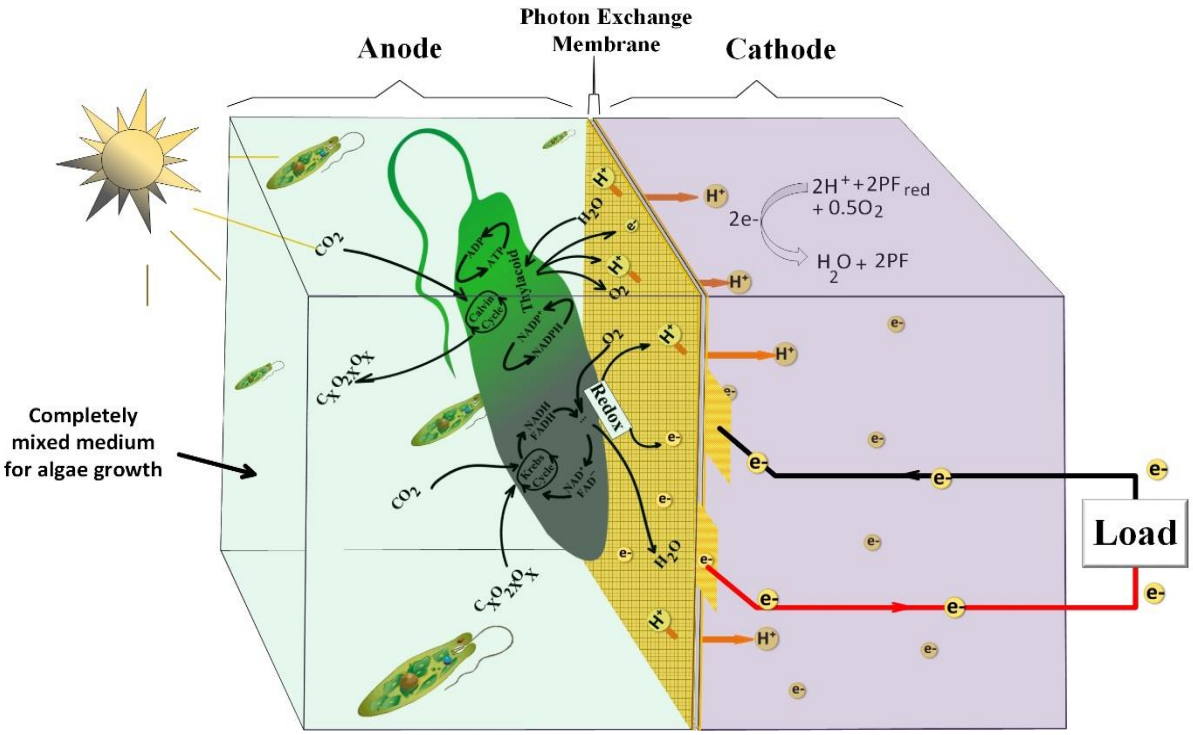

Fig. 1.1 General operational overview µ-PSCs.

The cathode chamber is filled with an electron acceptor described here as catholyte (solution in the cathode chamber) such as Potassium ferricyanide (PF).

$$4PF_{red} + 4H^+ + O_2 ==> 4PF + 2H_2O \qquad (1.7)$$

The Potassium ferricyanide is reduced by accepting electrons from the external circuit. The reaction is described as follows:

$$PF + e^{-} ==> PF_{red} \quad or \tag{1. 8}$$

$$F_e(CN)_6^{3-} + e^{-} ==> F_e(CN)_6^{4-}$$

Nafion is used as the proton exchange membrane (PEM). Highly conductive materials such as gold are sputtered on the surface of the PEM in order to collect the electrons liberated during respiration or photosynthesis of the green algae. The collected electrons on the surface of the PEM are sent through the external path through a load to the cathode chamber. The electrons recombine with the protons in a reaction with Potassium ferricyanide as described in equations *(1. 7)* and *(1. 8)*. The work in [6] provides deep information on the fabrication of the µPSCs and provide parameter studies based on practical results.

1.2.2 Output power capabilities of µPSCs

The extensive literature review conducted revealed that the researchers brought the µ-PSC technology to the maximum power generation ability of 400 mW/m^2 with up to 0.9V open circuit voltage (OCV) recorded in [7].

Fig. 1.2 shows the open circuit voltage of the fabricated µPSC during its early operation stages (first µPSC test after fabrication). No nutrients are added to the anode chamber. Also, the normal condition of temperature and pressure can be assumed.

Fig. 1.2 Sample testing in the laboratory.

The Polydimethylsiloxane (PDMS) material known for its properties of being optically clear, inert, non-toxic, and non-flammable is used for the µPSC envelope fabrication. A thin glass is used to cover the anode chamber as well as the cathode chamber. This aims to facilitate the light penetration in the reaction chamber for photosynthesis.

1.3 History of µPSCs technology

Research has been undertaken since the first µ-PSCs applications in the early 1990s. An overview of the recent research trend shows the focus on the improvement of the µ-PSCs using different micro-organisms [8] and [9], or membranes [10]. Some works focused on modeling and predicting the output of µ-PSCs ([11] and [12]). In these works, chemical and physical reactions inside the anode and cathode chambers are dynamically modeled taking into account the loading effect. The electrochemical equations used are based on kinetic equations and the predicted output is compared with the practical results.

Other works such as [13] and [14] were based on several tests on fabricated cells. The test results obtained provided some insights on the effects of some parameters on the power output from μ-PSCs. Practical tips to extract more power from μ-PSCs are given based on observations. Also, practical observations on the relation between day-night cycles and power generation were made. In [13], experiments are made using cyanobacteria in order to investigate the factors affecting the power generation with μ-PSCs. The experimental results obtained by applying 2 hours light and 2 hours dark conditions to the cyanobacteria proved the sustainability of the μ-PSCs technology. This work also revealed that minor changes in the temperature have no effect on the output of the power cell. The day and night energy production using μ-PSCs is investigated in [15]. Two different microorganisms are used in the reaction chamber in order to catalyze glucose during the day cycle and to produce electrons. This work investigated the effect of irradiation in the operation of μ-PSCs and concluded that the irradiation is an important factor that should be controlled for an efficient operation of μ-PSCs. Furthermore, this work proved the relationship between the irradiation and the operation of μ-PSCs. Also, the effects of the glucose and mediator concentration were studied and found to be directly related to the power produced by μ-PSCs.

The electrochemical modeling of μ-PSCs requires a better understanding of the chemical reactions occurring in the μ-PSC chambers also the process involved in the electrons liberation; source of electric power. All this starts with a better understanding of the unicellular organism growth and operation principles. Several works such as in [14] were undertaken in order to model the algae growth and the parameters intervening in the algae growth process. Basic and fundamental equations were then developed to represent

the algae. The work in [2] proposes a simple mathematical model describing the basic operation of μ-PSCs. The developed model assumed that the photosynthesis process is dominant over respiration. This enabled the elimination of the respiration process in the model. Based on this assumption, the developed model is validated for its ability to predict μ-PSCs performance. The parameters used in the resolution of the equations were mostly taken from previous works reported in the literature. Despite the assumptions made, the practical current-voltage (I-V) in steady-state results are found to match with prediction.

The technology improvement provided better and accurate electrochemical models taking into consideration the parameters involved in algae growth [16] - [19]. The factors affecting the algae growth have been investigated separately as well. In the work proposed in [20], the response of algae with respect to temperature, light and the photoinhibition was already of concern. They modeled the algae productivity by characterizing their photo inclination. In order to provide an accurate algal photosynthetic description, a brief incubation was conducted in order to reduce the number of required parameters in the photosynthesis-light intensity (P-I) equations. This method provided acceptable data describing the P-I relation for algae. In [21], the study of the light intensity in relation with the algae growth cycles revealed that the light intensity is effective only on the pre-commitment phase, a phase during which the cell commits to the division. They found that the light intensity increases the length of the pre-commitment phase and has no effect on the post-commitment phase. The Lambert formula was used to describe the incident light intensity. Also [22], highlighted the importance of including the effect of the light and temperature in the algae growth model. Light intensities and cycles are included in the electrochemical representation using Type II approach (Type II models predicts the

productivity of the entire culture by summing local productivities within the cultivation) both for the sake of simplicity and as a tradeoff between simplicity and practicability to simulate the outdoor environment and its effect on the algae cultivation.

The temperature effect on algae growth is investigated in [23]. Green algae, *Chlamydomonas reinhardtii*, was studied in order to determine its growth cycles and the relation between temperature and growth. It was grown under alternating light and dark cycles along with the variation of the temperature from 15-37 C. The time of the illumination period was found to be an important factor in the determination of the growth cycle of *Chlamydomonas reinhardtii*. Experiments designed in this work proved that the growth rate of the algae is proportional to the length of the cell cycle no matter what is the growth condition combination. This work also concluded that temperature is independent of the day/night cycle periodicity close to 24h with the living temperature range of *Chlamydomonas reinhardtii*. The studies conducted in [24], and [25] confirmed the importance of temperature as a factor affecting photosynthesis and respiration. These studies concluded that photosynthesis to respiration relation (P/R) is inversely proportional to the temperature. Above the optimum temperature for photosynthesis which is around 30 to 40 C, depending on the type of microorganism used, the respiration rate is almost doubled.

Some works focused on the combinational effect of the light intensity, nutrients addition, and oxygen on the photosynthesis. The work proposed in [26], and [27] suggested optimal periods of illumination for algae growth, by studying the effects of light/current

output relationship in μ-PSC and other plants. The proposed optimal periods of illumination are between 11 to 16 hours.

Other researchers took the topic into another dimension by modeling and representing the electrochemical equations of the μ-PSCs into equivalent circuits. This is the case in [28] where electrochemical equations are used in the electrical equivalent circuit representation. This work provided real-time understanding of the loading effect on the operation of the micro photosynthetic power cell. The equations accounting for anodic and cathodic reactions have been described and implemented in the electrical equivalent circuit. The transient and steady-state results obtained were close to the practical data obtained from a fabricated μ-PSC. However, the model did not consider the effect of the day/night, the pH and the temperature on the growth process of the cells. Also in this work the assumptions made considered the photosynthesis rate to be higher compared to respiration. Therefore the model accounted only for day growth of the cells. Also, the temperature was considered to be constant throughout the day.

1.4 Thesis motivation

Generating power from a living microorganism is a promising domain of research for the development of next generation environmentally friendly energy sources. The energy produced by μ-PSC can be used to power low power devices especially in remote locations. The maintenance cost for this eco-friendly technology is negligible compared to other renewable energy sources. However, the production cost along with its process are expensive and long and requires mature technology and specific materials. A trial and error method in the fabrication process optimization should be eliminated. This should reduce

the development and prototyping cost. Real-time accurate testing equipment should be available to ease the testing of μ-PSCs. The test results obtained should constitute a database from which the equivalent circuit model can be accurately developed for the simulation of the μ-PSCs. Also, along with the electromechanical design process, electrical aspects should be considered in order to provide means to extract power from this environmentally friendly energy source. For this purpose, the required electrical equipment should be developed for accurate power readings and estimation. Also, the required equipment should be inexpensive and have a fast acquisition ability in order to help understand, extract the power and model the dynamical behavior of the μ-PSC. These features are not found in practical ultra-low sensing circuits for currents. The available ones are complex and costly or are not able to provide dynamic testing of μ-PSCs.

1.5 Thesis objectives and scopes

The main objective of this thesis is to develop tools for testing, simulating and harvesting the energy from μ-PSCs. A real-time current sensing circuit covering the current output range of actual μ-PSCs is designed, prototyped and tested. The real-time sensing feature aimed to help researchers visualizing the effect of each element (temperature, micro-organism, membrane, pH, irradiation…) involved in the energy generation process of μ-PSCs. This thesis aims also to provide an understanding of the operation of μ-PSCs by improving the electrochemical equivalent circuit of μ-PSCs. The improvement will focus on the inclusion of the irradiance, day-and-night, pH, and temperature effects on the operation of μ-PSCs. The developed model will be validated and therefore can be used for

the simulation of μ-PSCs. Furthermore, in order to shift the μ-PSCs technology to the practical field, an energy harvesting circuit will be designed, prototyped and tested.

1.6 Organization of the thesis

This thesis will mainly focus on the electrical aspects of μ-PSCs technology. In chapter 2, a current sensing circuit is proposed. The proposed design will take into consideration the actual power range of μ-PSCs (μW to mW) and provides an accurate and real-time measurement of current from the cell. The circuit will be prototyped and tested with the fabricated μ-PSCs and with a low-power solar panel. In chapter 3, an improved electrochemical equivalent circuit of μ-PSCs is proposed and validated. This chapter will focus on the integration of the irradiation, the day and night cycles, the pH, and the temperature in the reaction chamber into the electrochemical equations describing the operation of μ-PSCs. It also presents the improved model in an electrical equivalent circuit form in order to simulate and evaluate the performance of the μ-PSC and predict the operation under maximum power transfer. A practical energy harvesting circuit for μ-PSCs is designed, prototyped and tested in chapter 4. The overall conclusions and future works are presented in chapter 5.

Chapter 2: Monitoring circuit design

2.1 Introduction

The motivation behind the development of a monitoring circuit can be summarized by the fact that practical ultra-low sensing circuits for currents are complex and costly or are not able to cover the range of operation of μ-PSCs (mA-nA). Also, the need for a dynamic monitoring circuit having a wide sensing range for the energy harvesting circuit can be considered as another motivation.

A literature review shows that many current sensing circuits have been proposed for ultra-low power applications. An overview presented in [29] concludes that Hall-effect sensors are the most suitable sensors meeting bandwidth, power, and low loss requirements. However, most of the proposed current sensing topologies are amplifier based. In order to resolve issues related to an amplifier based current sensing, a circuit which consumes low power and less susceptible to temperature variations is proposed in [30]. The proposed design in [30] reduces the silicon area and has an increased resolution, however, it cannot be used for ultra-low current sensing applications. Also, some designs considered the precision resistor in the amplifier based sensing circuits by proposing a combination of resistors for good accuracy such as in [31]. In [32], an integrated circuit with capacitive feedback trans-impedance amplifier is proposed. The results obtained are acceptable, however, the range of the topology is narrow. A wide range ultra-low current sensor is designed in [33]. It is able to sense currents from a few femtoamperes (fA) to microamperes (μA). The circuit is built with an external switch and capacitor. This can affect the dynamic behavior of the circuit and with difficulty in meeting our design requirements.

The proposed current sensing circuit takes into consideration the actual power range of μ-PSCs. It also provides an accurate measurement with its simple design and implementation. The digital readout provides the reading over the full voltage and current range instantaneously. This integration should help researchers in the understanding of the full operation of the cell. This will also enable them to create a database of the test results automatically instead of manually recording only some points in the I-V curve.

2.2 Principles of operation

The proposed current sensing circuit has both analog and digital circuit sections. Both of them are combined in the same design to provide full range reading and storage capability enabling a full current range scan for μ-PSCs.

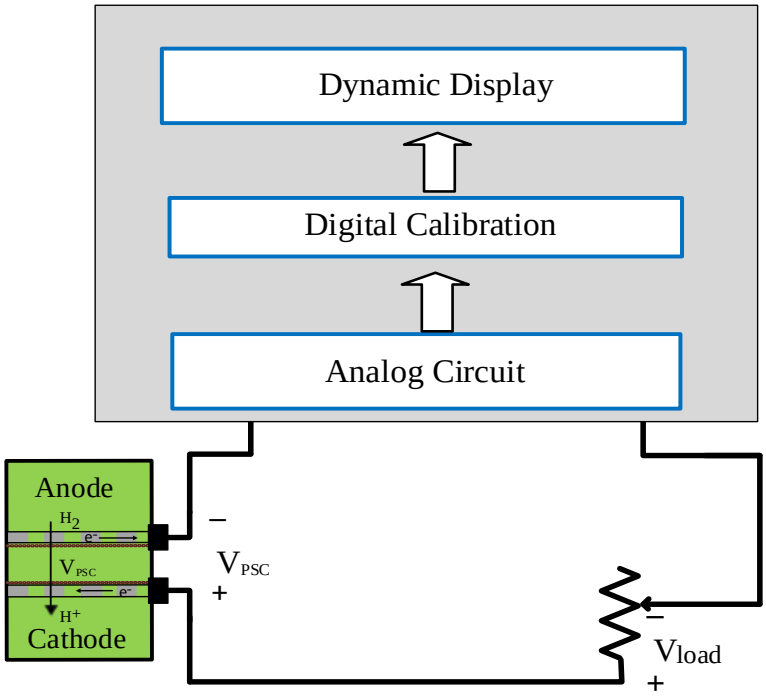

Fig. 2.1 Proposed dynamic current sensor.

2.2.1 Analog section

An ideal current sensing method should not create any disturbance in the current being sensed. The design concept of this current sensing circuit can be considered as a variant of the Hall-effect sensor if one considers the virtual loops in *Fig. 2.2*. In fact, it is based on the current to voltage converter concept. Two negative feedback connected operational amplifiers (op-amps) are used to provide a reference and also a virtual ground to the circuit shown in *Fig. 2.2*. Both of them are high precision op-amps. The first op-amp serves as a reference to the output signal V_o during the analog to digital conversion process. This avoids negative voltages at the analog to digital converter (ADC) terminals. The second op-amp is the actual current sensing part of the circuit. The current to voltage conversion process takes place across $Rcal$. Based on the negative feedback properties of the op-amp, V^+ and V^- are at the same potential. The op-amps are driven directly from the Universal Asynchronous Receiver/Transmitter (UART) port. This provides an independent operation of the sensing circuit without affecting the current being driven from the μ-PSC. Therefore the proposed sensing circuit is comparable to the self-powered digital ammeter with dynamic output capability. The difference between the proposed topology and normal current to voltage converters is the reference setting block for the analog section. Based on the range requirements, the value of V_{ref} and/or V_{cc} can be adjusted. The simplicity of the design makes the adjustment of V_{ref} directly related to R_{cal_1}.

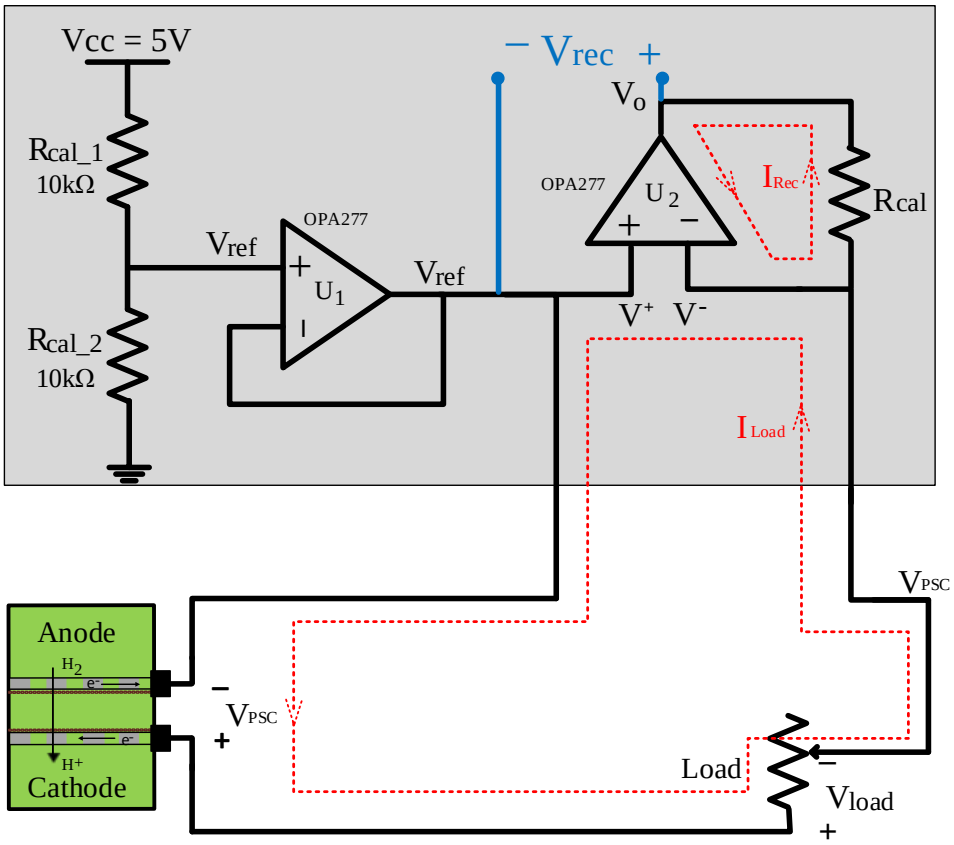

Fig. 2.2 Analog dynamic current sensor ***(Currents paths are virtual and are only used to illustrate how the sensing circuit is close to the Hall-effect sensor. No currents flow into/out of the op-amps input terminals).***

Micro-photosynthetic cells behave like constant current sources at low voltage, similar to the solar cells. This characteristic from µ-PSCs provides full operation of the proposed current to voltage concept based sensing circuit. The current from the µ-PSC flows through the load and virtually returns back to the source assuming an ideal op-pamp connected in negative feedback and therefore,

$$V_{PSC} = V_{load} \tag{2. 1}$$

Practically there is a leakage current of the order of picoamperes at the input terminals of the op-pamp because of its finite input resistance. However, this leakage current has no

effect on the current being sensed thanks to the calibration process in the digital section of the circuit (see *Fig. 2.3*).

The current, therefore, because of the very large input resistance of the op-pamp, will flow through $Rcal$. The output voltage can, therefore, be expressed as:

$$V_o = V_{ref} - I_{rec}R_{cal} \quad (2.\ 2)$$

$$V^+ = V^- = V_{ref} \quad (2.\ 3)$$

The configuration in *Fig. 2.1* provides a current reading without degradation of the result. Based on the precision of the practical results obtained (see *Table 2.1*), no extra components are required to correct the readings. A ±1% tolerance resistor is selected for R_{cal}. The selected high precision op-pamp is OPA277P. The OPA277P is an improved noise elimination amplifier with a wider output voltage swing (±2 V to ±18 V). It is twice as fast with half the quiescent current of a 800 μA/amplifier. It has an ultralow offset voltage of 10 μV, a voltage drift of ±0.1 μV/°C, and a low bias current of 1nA maximum. The common-mode rejection of this op-amp is as high as 140 dB with a high power supply rejection of 130 dB [34].

The reading error observed is directly related to the precision of R_{cal} (±1%). The error related to the non-linearity of the op-amp is solved in the digital section using the calibration factors obtained with practical tests.

2.2.2 Digital section

In order to provide a dynamic reading and data recording ability to the proposed sensing circuit, a microcontroller is used in the circuit. As shown in *Fig. 2.1*, the digital operation starts with an analog to digital conversion (ADC). The output voltage from the current to

voltage conversion through R_{cal}, is referenced to V_{ref} in order to make the input voltage to the ADC always positive.

$$V_{rec} = V_{ref} - V_o \tag{2. 4}$$

$$V_{rec} = I_{rec} R_{cal} \tag{2. 5}$$

From equation *(2. 5)* R_{cal} is as a current gain. Therefore by adjusting R_{cal} one can easily change the current range without impacting the normal operation of the circuit. In this design only one value of R_{cal} is set for mA, µA, and nA ranges. Practically without the calibration, the readings will lose the precision because of the wide range under consideration. The digital part is therefore designed with the algorithm below to calibrate the reading.

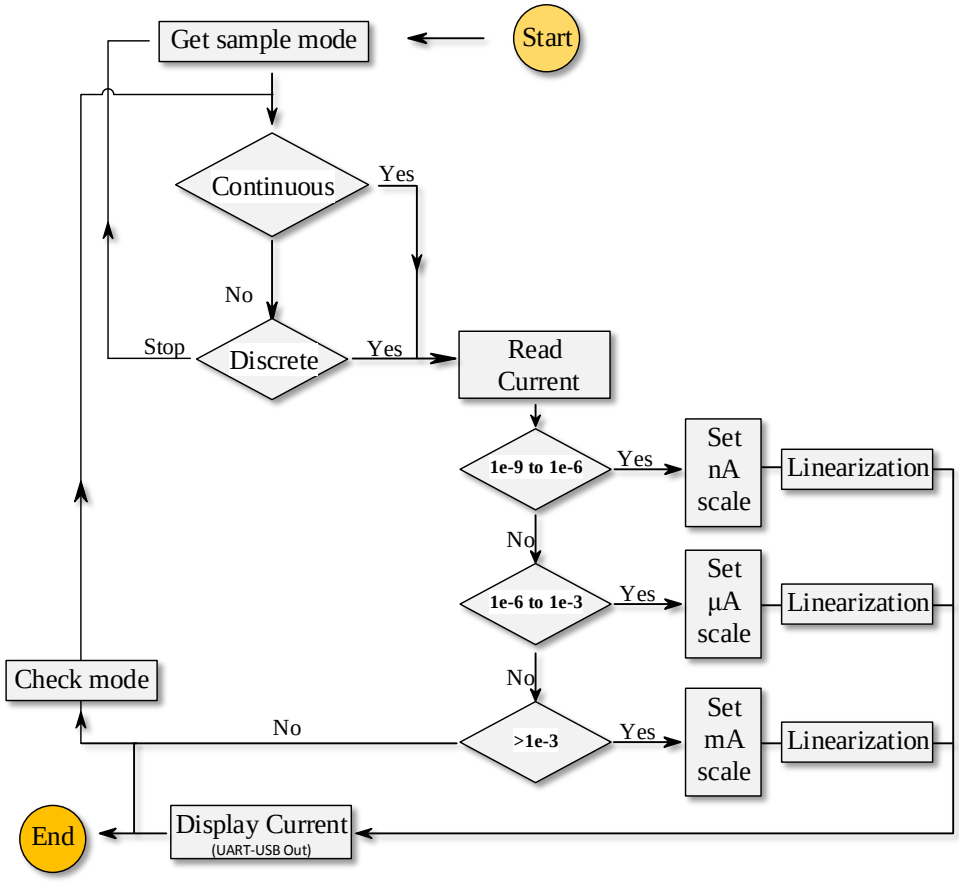

Fig. 2.3 Calibration algorithm.

This algorithm enables continuous sampling and discrete sampling of the currents being sensed. Since the voltage from the actual μ-PSCs is generally in the range below 1V, the results are accurately digitalized and therefore do not need calibration. The calibration of the current is prioritized for accurate reading over the specified ranges. The current calibration feature enables this current sensor to be accurate over the current range of actual μ-PSCs. The aim is to facilitate a full investigation on the power range of the μ-PSC and provide accurate results for a deep understanding of the effects of each factor implicated in μ-PSCs operation. Thanks to the data acquisition speed of the microcontroller (118.75 ksps max) and the digital filtering included (delta-sigma ADC), A high-resolution digital output is obtained with reduced quantization error noise. The recorded data is then confined in a range for better precision adjustment using a linearization block. The linearization block sets a scaling factor specific to the range in order to correct the measurement. The scaling factors for each range are obtained from several measurements and comparison between the sensed current and the practical values of the current. Practically, The ADC is set to 20 bits of resolution with a sample rate set at 187 samples per second (SPS).

The UART serial communication module in the microcontroller is used to send the sensed current along with its range to the computer for dynamic display and recording via a USB port. Also, the microcontroller circuit provides the power to the sensor circuit. No separate power source is required for the sensing circuit. *Fig. 2.4* shows the prototyped sensor.

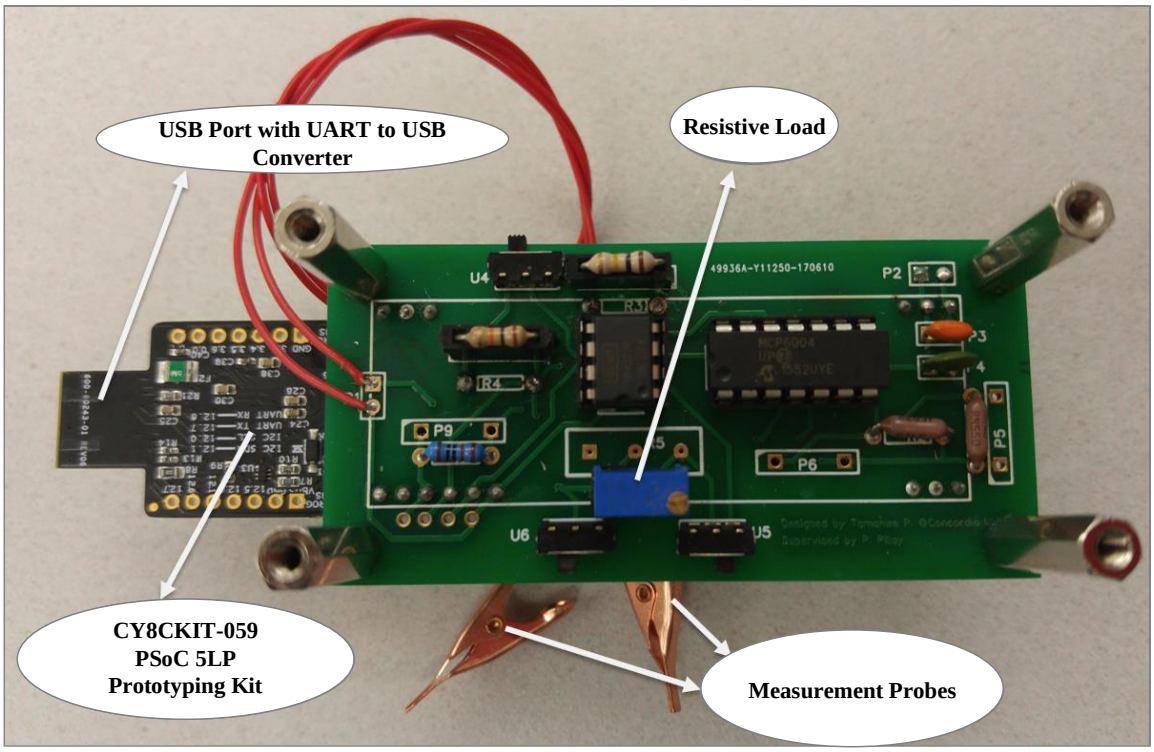

Fig. 2.4 Real-time current sensing circuit prototype.

2.3 Results

2.3.1 Accuracy test process

In order to verify the accuracy of the proposed current sensor, a wide range of current data starting from the nA range up to 1 mA are acquired with the sensor and compared with the measured data.

The experimental setup in *Fig. 2.5* comprises a variable voltage source for the emulation of the cell. The precision digital multimeter Fluke 289 is used for the calibration. The dynamically recorded current is displayed on the screen using Putty software.

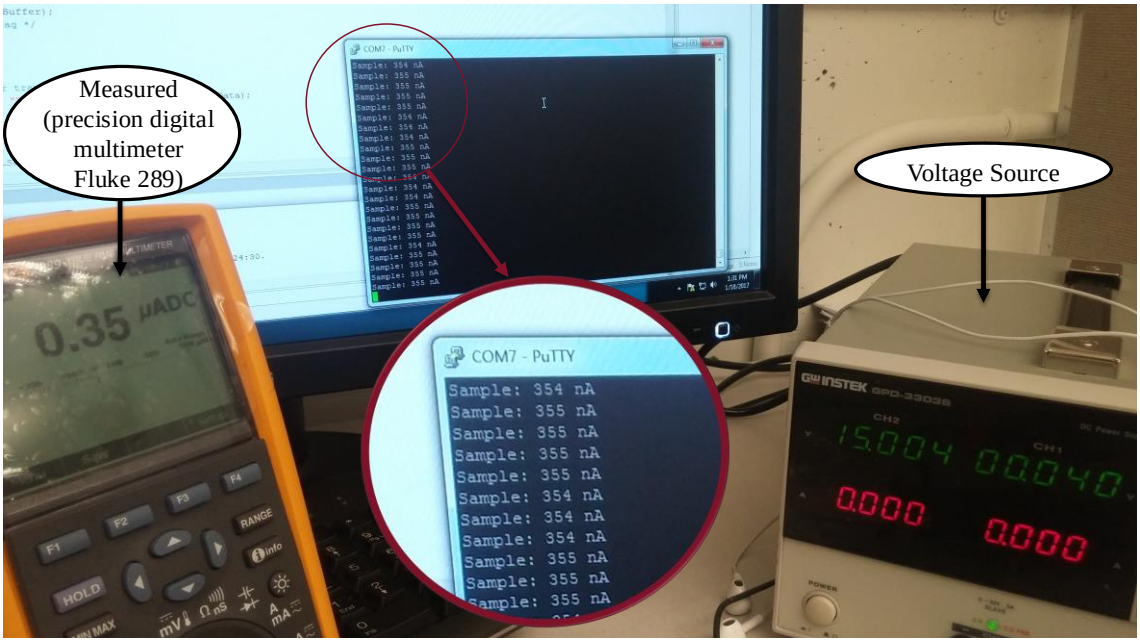

Fig. 2.5 Experimental setup for sensing circuit calibration.

Some of the practical results obtained are shown in *Table 2.1*. It can be seen that the proposed current sensing circuit has an acceptable accuracy especially in the nA range and covers a wide range of current measurement suitable for the u-PSCs.

Table 2.1 Error calculation

	Measured	***Sensed***	***Absolute error***
Current(µA)	0.01	0.01	**±0%**
	0.05	0.05	**±0%**
	0.15	0.15	**±0%**
	0.35	0.35	**±1%**
	1.73	1.74	**±1%**
	7.38	7.39	**±1%**
	117.10	117.09	**±1%**
	589.58	589.59	**±1%**

2.3.2 Dynamicity test of the sensing circuit

The operation of the sensing circuit is depicted in *Fig. 2.6* and *Fig. 2.7* by varying the load (variable resistor). A low power solar panel is used for testing and for reference purposes since photovoltaic systems are a mature technology.

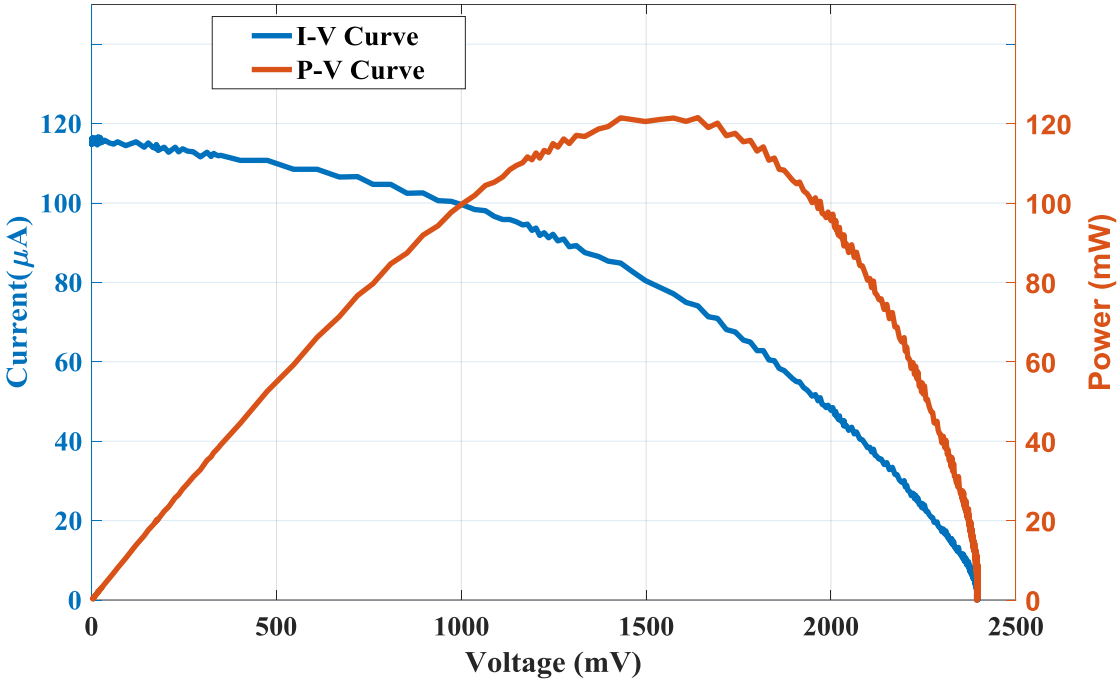

Fig. 2.6 I-V, P-V characterization of a solar panel using variable resistive load.

The obtained result with the μ-PSC is shown in *Fig. 2.7*. It gives more details regarding the dynamics of the μ-PSCs. The visible notches on the I-V and P-V curves in *Fig. 2.7* can be attributed to the nonexistence of a storage element in the sensing circuit. However, they may be also part of the characteristic of the μ-PSCs. Practically recorded data in [28] had also some notches. Furthermore, more investigations should be made in order to understand the existence of that notch. For proper I-V and P-V relation visualization, some

works proposed the use a dc to dc converter as a load for a smooth operating points scan. However, this is not within the scope of this work. The dynamic behavior of this sensing circuit can be observed with a step load change which validates the ability of this sensing circuit to provide a better understanding of the dynamics involved in the µ-PSC operation without the need for expensive testing equipment.

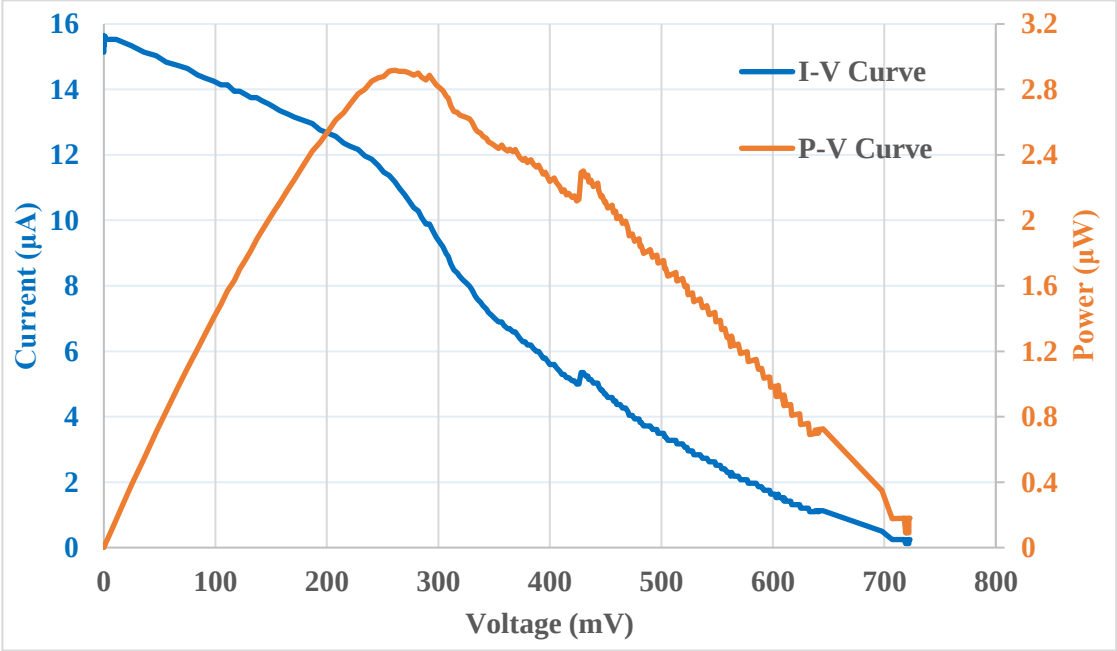

Fig. 2.7 I-V, P-V characterization of a µ-PSC using variable resistive load.

2.4 Conclusion

A current sensing circuit is designed, prototyped and tested for use in the characterization of a µ-PSC. The readings obtained are dynamic and accurate up to the second digit in nanoampere range. The prototyped circuit is used to record dynamic data from the µ-PSC and was able to cover the full power range without loss in accuracy. It can

help obtain a better understanding of the dynamics involved in power generation from a μ-PSC. Also, the effect of each parameter on the photosynthesis and electrons liberation in the reaction chamber can be easily investigated for improvement purposes of the cell and also of the electromechanical model of μ-PSCs. This sensing circuit will be used in chapter 4 for the energy harvester's maximum power tracking circuit implementation.

Chapter 3: Improved μ-PSC model

3.1 Introduction

This chapter focuses on providing a tool for the simulation of μ-PSCs. The simulation tool which is the equivalent circuit representation of μ-PSCs is based on the integration of the irradiation, the day and night cycles, the pH, and the temperature in the reaction chamber into the electrochemical equations by combining work done by other researchers from different fields. It also presents the improved model in an electrical equivalent circuit in order to simulate/emulate and evaluate the performance of the μ-PSC and predict the operation under maximum power transfer. The electrochemical equations will be updated based on recent research results in chemical, electrical, and biological fields on μ-PSCs followed by a circuit level representation of μ-PSCs.

3.2 Models

3.2.1 Previous designs limitations

From the work done by electrical engineers, chemical engineers and biologists this thesis comes up with an updated model for the μ-PSCs. The equations developed are mostly taken from the electrochemical equations describing the operation of μ-PSCs as proposed in [2], [3], [7] and [28]. The assumptions in previous works include:

1. Parasitic reactions neglected
2. Uniform concentration of gas and nutrients
3. Uniform distribution of microorganisms
4. Cell growth described by double Monod kinetics
5. Membrane is impermeable to sugar, and other nutrients.

6. Negligible activation losses
7. Butler-Volmer equations for electrodes representations
8. Constant number of photons absorbed by each cell
9. Constant irradiance
10. Constant temperature and pH and pressure
11. Photosynthesis is more dominant
12. Instant state change of gas to liquid

With the above assumptions, acceptable results and estimates were obtained but there is a possibility for improving the model. An improved model reducing the number of assumptions is presented in this work. The assumptions from 8-12 are eliminated by including them in the developed equations.

3.2.2 Updated model parameters

i. Growth and death rate of algae cells

The algae growth is related to several factors such as nutrient availability, irradiation, day and night cycles, temperature, pH etc.

From the work proposed in [18], the algae growth can be modeled as follows:

$$\frac{dN_{cell}}{dt} = K_1 A_c N_{cell} - K_2 N_{cell} \quad (3.1)$$

N_{cell} (g/m^3) is the number of living cells.

K_1 (1/sec) is the growth rate of cells; highly dependent on the nutrient used in algal growth in the chamber.

K_2 (1/sec) is the death rate of cells.

A_c is the attenuation constant which is function of light intensity, system temperature, nutrients availability, the day and night cycles and the pH of the solution.

The relations and interdependence of all these factors are studied in [22] by using different approaches. However, the model proposed in [18] is more practical. It considers the type I approach which just multiply the effects of each factor to get the attenuation constant.

ii. Light intensity effect of algae growth

The influence of the intensity of light on the algae growth is modeled in [16] and [18]. However, the model in [18] is found to be more accurate as shown in the equation below.

$$P\ (I)\ =\ 9.34\ (1-\ e^{(-0.0044 I_{avg})})\ -1.60 \qquad (3.\ 2)$$

$P\ (I)$ is the light intensity.

$I_{avg}(W/m^2)$ is the average light intensity. It is a function of incident light intensity, depth of the anode chamber, day and night cycle, and algal turbidity. The light intensity model is based on Beer-Lambert equation described as,

$I = I_\beta e^{-eD}$

$I(W/m^2)$ is the light intensity, D is the anode chamber depth. I_β and $e(1/m)$ are respectively the day and night cycles of the algae growth, and the total extinction coefficient.

iii. System temperature effect on the algae growth

Parallel to previous models that considered the temperature to be a constant or having negligible effect on the practical results, the equations developed recently in [16], [18] and [22] modeled the temperature dependency of the algae growth using equation *(3. 3)*.

$$P(T) = e^{-K_{TEC}(T-T_{OGT})^2} \quad (3.\ 3)$$

$P\ (T)$ is the system temperature.

K_{TEC} is temperature effect coefficient ($1/K^2$).

T is the temperature of the anode chamber (K).

T_{OGT} is optimal growth temperature of the selected algae (K).

iv. Nutrient availability and algae growth

Depending on the type of microorganism used in the reaction chamber, the number and type of nutrients may vary. However, the basic nutrients such as sugar, nitrogen, carbon dioxide and phosphate are modeled with Monod equations in [18] as follows:

$$\frac{dN_x}{dt} = -K_x r_x A_c N_{cell} \quad (3.\ 4)$$

N_x is the nutrient availability, x (g/m^3).

K_x is the rate of change constant of nutrient x.

r_x is the consumption rate of nutrient x.

v. pH of the solution and algae growth

The pH of optimal algae growth varies depending on the algae species. However, the relation of the pH of the solution and the carbon dioxide concentration is constant and is characterized by the inverse proportional relationship described below [18].

$$P\ (CO_2)\ = \frac{1}{1+exp(\lambda(P^H - P^H opt))} \tag{3. 5}$$

$P\ (CO_2)$ is the CO_2 availability.

$P^H opt$ is the optimal growth pH of the selected specie of algae.

λ is the Lagrange multiplier.

3.2.3 Circuit level representation

The proposed equivalent circuit for μ-PSCs in [28] took into consideration some electrochemical reactions described in form of differential equations. The effect of irradiance, temperature and the pH of the solutions were not explicit in the formulation. Therefore the model was not able to predict the effect of alternating day and night cycles, irradiance, temperature and pH on the growth cycle of algae responsible for energy production in μ-PSCs. Based on equations *(3. 1)* to *(3. 5)*, the updated electrochemical model of μ-PSC can be represented as shown in *Fig. 3.1*. Factors affecting the algae growth, photosynthesis and respiration such as the irradiation, the day and night cycle, the temperature and the pH of the solution are not neglected.

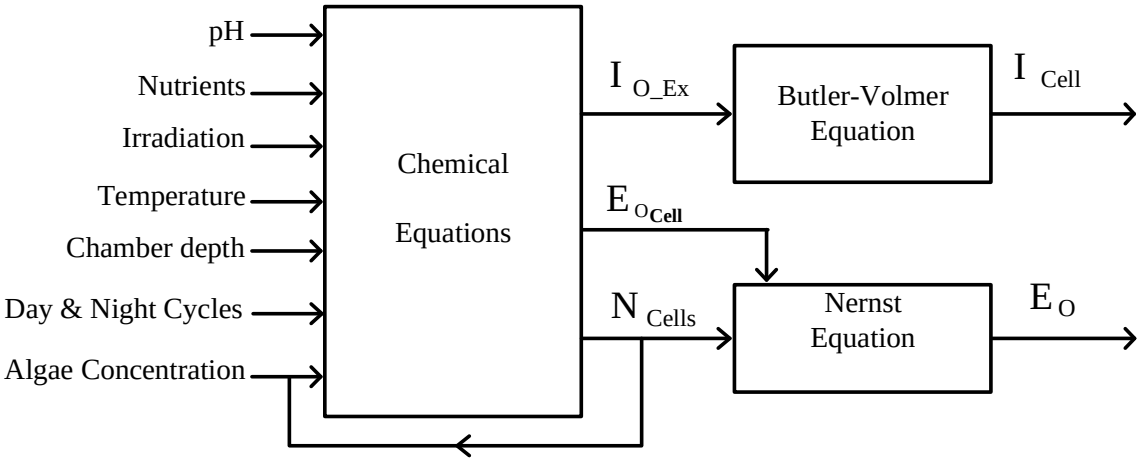

Fig. 3.1 Updated electrochemical model of μ-PSCs.

E_o(V) is the Nernst voltage described as the difference between the standard thermodynamic voltage Eo_{cell} and the voltage due to chemical reactions. It is derived from equations *(1. 2)* to *(1. 8)* following [35].

Rewriting equation *(1. 3)* we have:

$$2Med_{red} \ ==> \ 4e^- + 2H^+ + 2Med \tag{3. 6}$$

$$V_{an} = E^0_{anode} - \frac{RT}{4F} \ ln \left(\frac{[Med_{red}]^2}{[Med]^2[H^+]^2}\right) \tag{3. 7}$$

E^0_{anode} is the electromotive force due to standard redox potentials in the anode chamber.

Equation *(1. 8)* gives:

$$V_{cath} = E^0_{cathode} - \frac{RT}{4F} \ ln \left(\frac{[PF_{red}]^4}{[PF]^4}\right) \tag{3. 8}$$

$E^0_{cathode}$ is the electromotive force due to standard redox potentials in the cathode chamber.

The open circuit voltage is, therefore:

$$E_o = E_{o_{cell}} - \frac{RT}{4F}\, ln\, \left(\frac{[Med_{red}]^2[PF_{red}]^4}{[PF]^4[Med]^2[H^+]^2}\right) \quad (3.\ 9)$$

$E_{o_{cell}} = E^0_{anode} - E^0_{cathode}$ is the electromotive force of the cell due to standard redox potentials. It can be as high as 1.241V [2]. However, the cell potential E_o is previously developed in [36] and found to be in the range between 0.953V to 0.991V. This result is also proven in [4] where E_{o_cell} is found equal to 0.965V.

The output voltage under any given load can be described following [19] and [35] as in equation *(3. 10)*.

$$V_o = E_o - (\sum V_{loss} + I_{Cell}R_s) \quad (3.\ 10)$$

$$\sum V_{loss} = \sum V_{loss\_an} + |\sum V_{loss\_cath}| \quad (3.\ 11)$$

V_{loss_an} and V_{loss_cath} are over potentials in the anode and cathode chambers.

The overpotentials at anode and cathode surfaces are mainly related to the concentration, activation and ohmic losses. Mass transfer losses also known as concentration losses are due the insufficient reactants or products from electrodes. Activation losses are the resultant of the energy losses during redox reactions initiation and during electron transfer. Ohmic losses result from the conductivity of the anolyte [35]. Equation *(3. 10)* becomes:

$$V_o = E_o - (V_{AL} + V_{CL} + I_{Cell}R_s) = R_L I_{Cell} \quad (3.\ 12)$$

V_{AL}(V) is the activation is losses.

V_{CL}(V) is the concentration losses.

R_L(Ω) is the external load.

R_s(Ω) the internal series resistance.

The concentration losses V_{CL} and the activation losses V_{AL} are closely related to the current density at the anode surface. They are expressed in [28] and [37]as shown in equations *(3. 13)* and *(3. 14)*.

$$V_{CL} = -\frac{RT}{\alpha F}\, ln\left(1 - \frac{I_o}{i_L}\right) \quad (3.\ 13)$$

$$V_{AL} = \frac{2RT}{nF} sin\, h^{-1}\left(\frac{I_o}{2i_o}\right) \quad (3.\ 14)$$

$$I\_o = \frac{I_{Cell}}{A_E} \quad (3.\ 15)$$

i_L(mA/cm^2) is the limiting current.

I_o is the current density expressed in terms of the equilibrium exchange current density.

i_o is the equilibrium exchange current density

α the effective charge transfer coefficient.

F is the Faraday's constant.

The equilibrium exchange current density i_o (A/cm^2) is described using Butler-Volmer equation [38] and [39] as shown in equation *(3. 16)*.

$$i_o = I_o \left(\frac{1}{exp\left(\frac{\alpha nF}{RT} V_{AL}\right) - exp\left(\frac{-(1-\alpha)nF}{RT} V_{AL}\right)} \right) \quad (3.16)$$

Where $A_E(m^2)$ is the electrode surface area. The exchange current density I_o is typically 0.001 A/m^2 [19].

The equivalent circuit based on the developed equations is shown in *Fig. 3.2*.

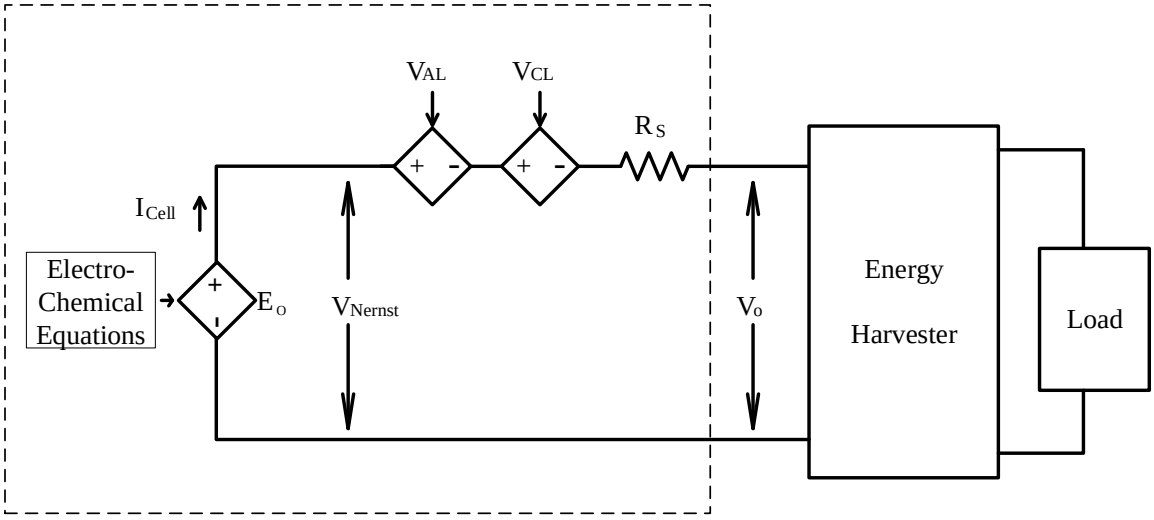

Fig. 3.2 Updated general equivalent circuit for μ-PSCs.

The output circuitry consisting of the energy harvester and load can be considered as load (R_L) for simplicity. Practically, for the case as illustrated in *Fig. 3.2*, the impedance as seen from the output of the μ-PSC should be considered as the load. In the simulation, a resistor is used as the load. The theoretical and practical I-V relationship of μ-PSCs can be summarized as shown in the *Fig. 3.3*. The characteristic curve describes also fuel cells ([40]). One can see the effect of all the losses on the output of the cell.

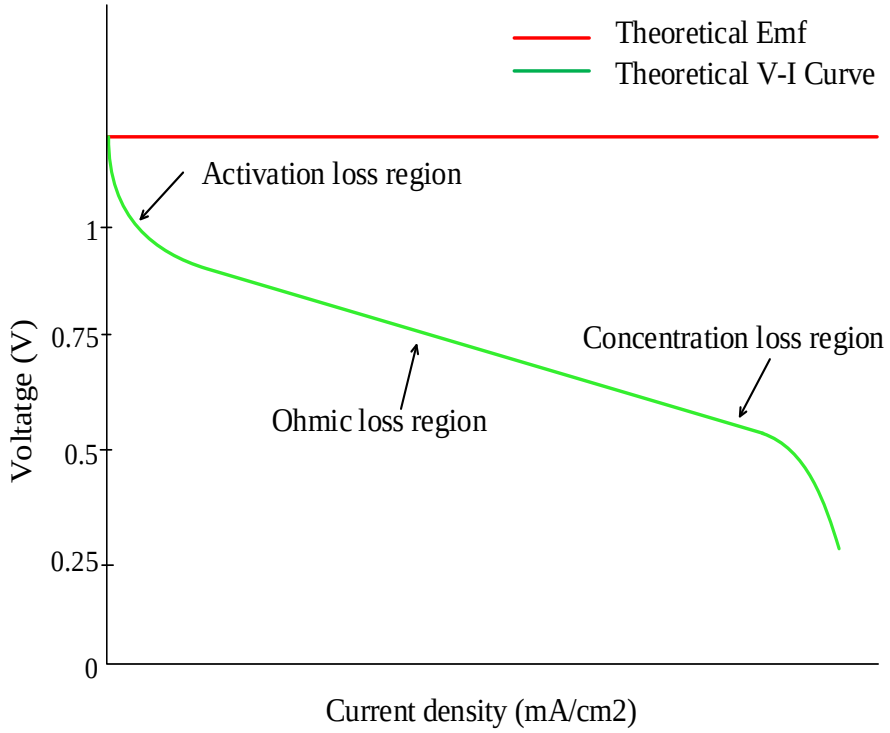

Fig. 3.3 Voltage-Current characteristic of μ-PSCs

Through this I-V characteristic, the loss mechanism in the μ-PSC can be easily understood. The main losses are activation and concentration losses due to overpotentials at the anode and cathode surfaces and also due to the mass transfer losses caused by insufficient reactants or products from electrodes or energy losses during redox reaction initiation and during electron transfer.

3.3 Model solution

Initial conditions used in the solution of the differential equations describing chemical reactions are listed in *Table 3. 1*. The model in *Fig. 3.2* is developed and simulated using MATLAB-Simulink assuming that the algae species used is *C. reinhardtii* CC-125 (ambient air at 25 °C, pH 7.0). The open circuit voltage at any instant of time is calculated

by subtracting the potential due to the chemical reactions from the electromotive force of the cell due to standard redox potentials as described in the equation *(3. 9)*. The block diagram is illustrated in *Fig. 3.4*. The irradiation is implemented by a simple sinusoidal function with negative cycle set to zero. The amplitude of the positive half cycle is adjusted in order to provide a variation in the irradiation level. Therefore, it also provides the day/night cycles to the growth of algae.

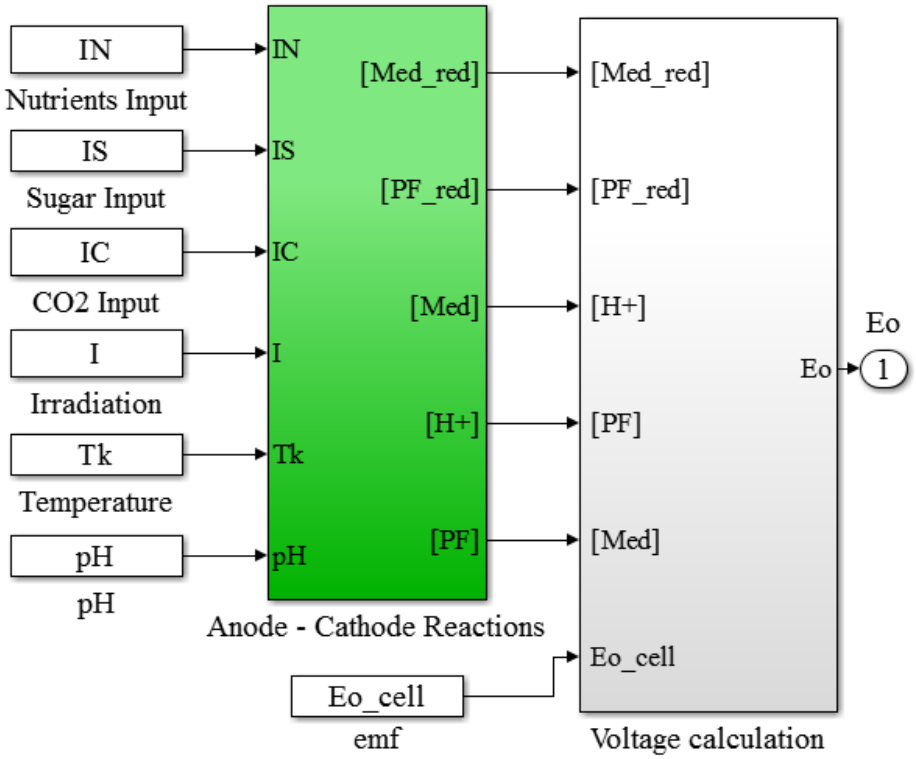

Fig. 3.4 Open circuit voltage calculation blocks for µ-PSCs. Open circuit voltage calculation blocks for µ-PSCs.

Table 3. 1 Model parameters

Symbol	Description	Value	Source
K_{TEC}	Temperature effect coefficient	0.0001	[18]
K_{TEC}	Optimal growth temperature	300 K	
E_{o_cell}	Electromotive force of the cell	1.241 V	[2]
R_L	External load	Variable	
R_s	Internal series resistance	599 Ω	[28]
i_L	Limiting current	0.182 mA/cm^2	[28]
I_o	Equilibrium exchange current density	0.001 A/m^2	[40]
X	Initial concentration of cells	12.2 g/m^3	Assumed
N	Initial concentration of nutrients	2890 g/m^3	Assumed
So	Initial concentration of sugar	10 g/m^3	Assumed
CO_2	Initial concentration of CO_2	7 g/m^3	Assumed
AE	Anode active surface area	4.84e-4 cm^2	[28]
Va	Volume of anolyte solution	2e-6 m^3	Practical
Med	Initial concentration of redox coupler	2923.5 g/m^3	Assumed
Med_{red}	Initial concentration of reduced redox coupler	1 g/m^3	Assumed
Ho	Initial concentration of hydrogen (protons)	1 g/m^3	Assumed
Vc	Volume of catholyte solution	2e-6 m^3	Practical
PF_{red}	Initial concentration of reduced catholyte	1 g/m^3	Assumed
PF	Initial concentration of oxidized catholyte	3e6 g/m^3	Assumed
pH	pH	7	[19]

3.3.1 Model characteristics

The solution of the developed model provided the well-known current-voltage (I-V) relationship curve for µ-PSCs. The I-V curve, *Fig. 3.5*, is obtained at 25 °C, 683.75 W/m^2, pH 7.

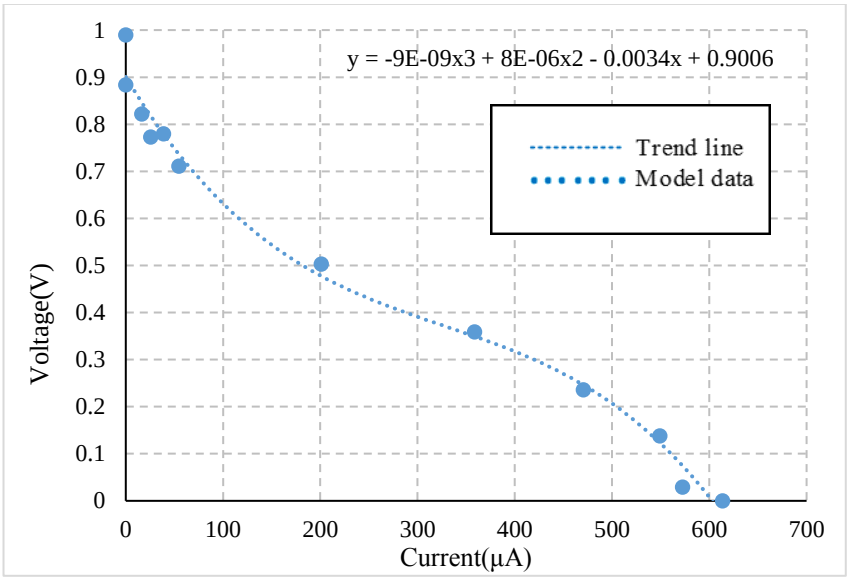

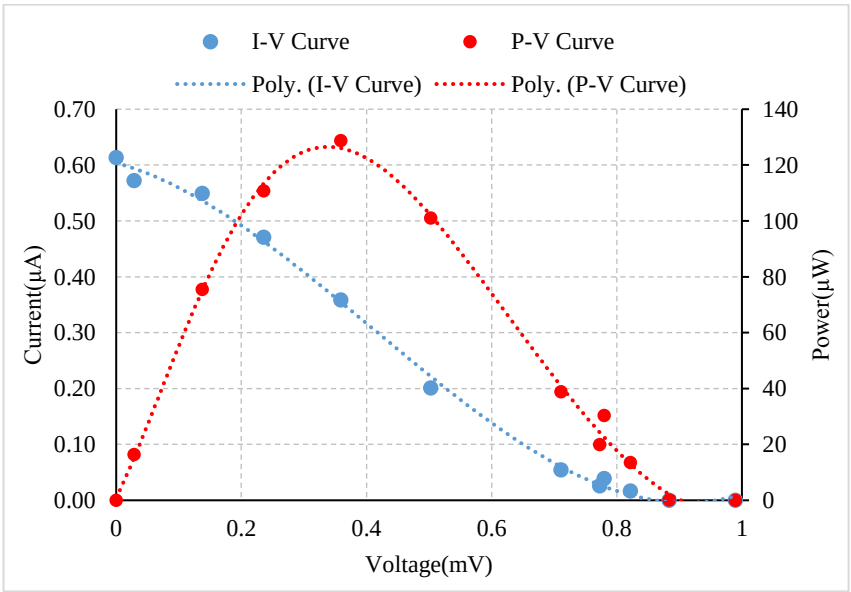

Fig. 3.5 Model characteristics of µ-PSCs (25 °C, 683.749 W/m^2 , pH 7)

3.3.2 Irradiance and dark/light cycles effect on the power production

The dynamic behavior of the model is depicted in *Fig. 3.6.* Here, the model is run under three different light intensities for a period of 10 days. For those different cases, the load was kept unchanged at 1kΩ. Also, the nutrients were provided on a regular basis. The output power curves, *Fig. 3.6-b*, show the existence of a relation between the irradiation and the output power of the cell. Also, they validate the light intensity effect on the algae growth (*Fig. 3.6-a*). A high level of irradiance increased the growth rate of algae assuming the nutrients are available and sufficient. However, it affects the output power especially during the exponential growth period of the cells. This can be attributed to the increased algal turbidity, the over-consumption of nutrients, and many other factors that can be investigated separately. The saturation period observed after almost 6 days shows that during the saturation, the output voltage (power) is no longer dependent on the irradiation level which is greater than the threshold irradiation required for photorespiration in the algae. Therefore, running the photosynthetic power cell under the dark condition for a long period of time will result in a curve similar to the one obtained with 150 W/m^2 illumination level and shown in *Fig. 3.6 a*, and *Fig. 3.6-b*. This is caused by the photo inhibition of algae growth.

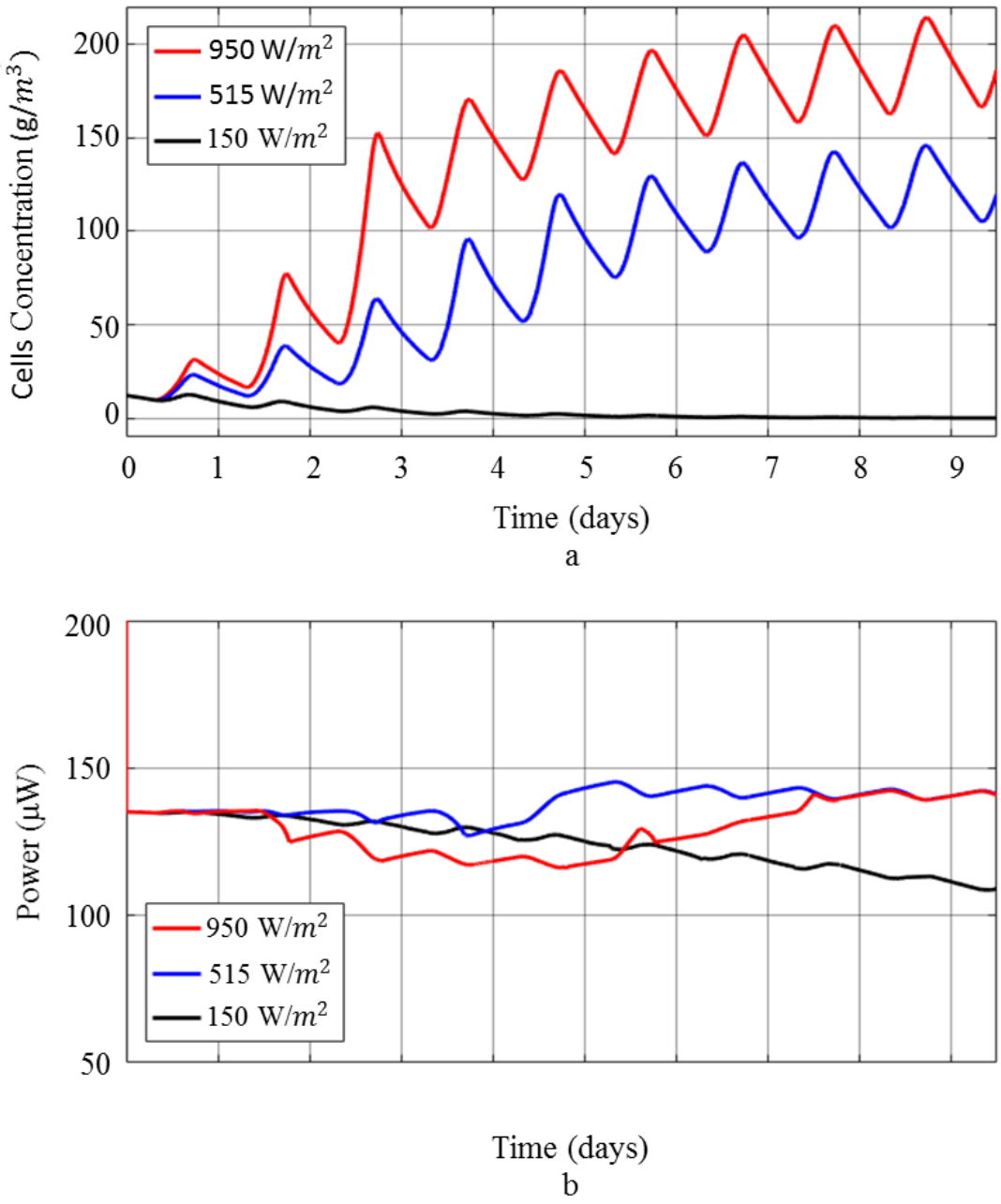

Fig. 3.6 Dynamics of µ-PSCs under different irradiations (25 °C, pH 7). a- Living cells concentration, b- Power output from the power cell.

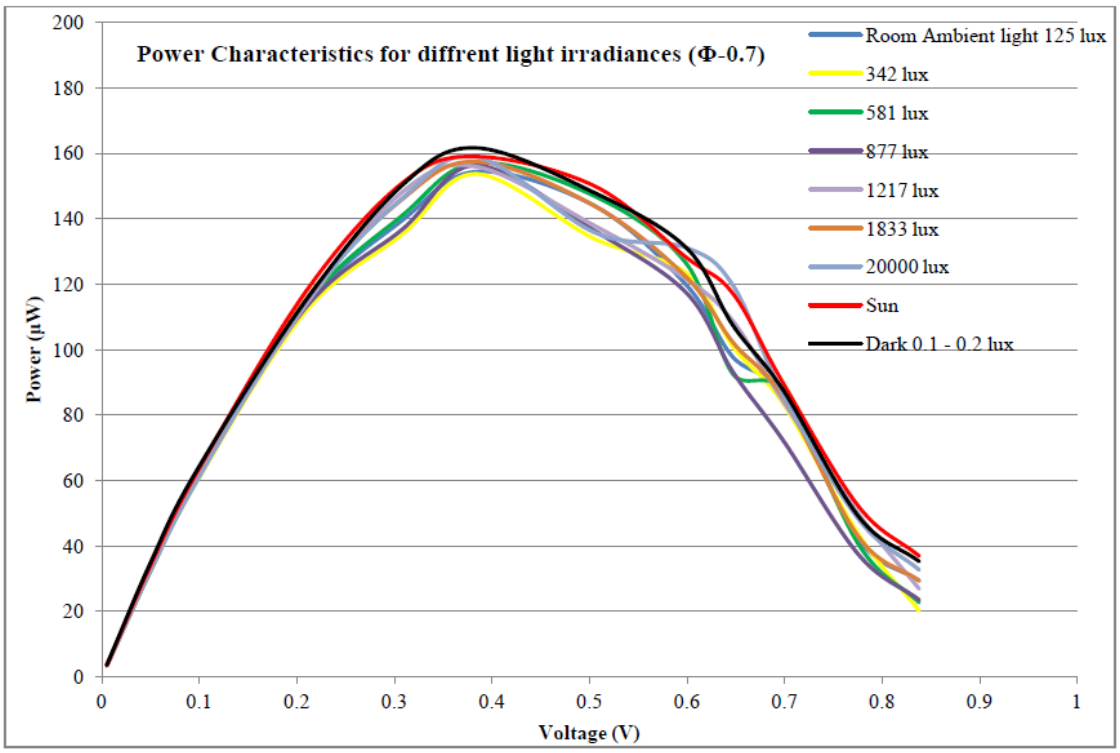

Fig. 3.7 Practical power characteristic curves of µ-PSCs under different irradiations [7]**.**

The power generated varies depending on the exposition duration of the cell to the light. For a short exposition time, the practical results previously obtained in [7] and shown in *Fig. 3.7* revealed a confusing relationship between the irradiation and the power output. This is because under "sun" and "dark" situations in *Fig. 3.7*, the power outputs are similar. In order to investigate the irradiation level-output power relationship, the PV curves are obtained after two light/dark cycles with the maximum irradiation level kept constant during this period. The same experiment is repeated several times by changing the maximum irradiation level for each new experiment. The results obtained are illustrated in *Fig. 3.8*. Optimal power generation versus light intensity is highlighted. One can see that very low/high irradiation levels contribute less to the output power. The maximum power output of the cell is in between the two extremes. In fact, both ranges (very low/high

irradiation levels) are limiting factors to the algae growth. The obtained results are similar to the practical results and deductions made in [23], [26], and [27] and hence validate the proposed model in terms of its ability to emulate irradiation and day and night cycles on the μ-PSCs operation. The optimal irradiation level may depend on the type of algae species used in the anode chamber as well.

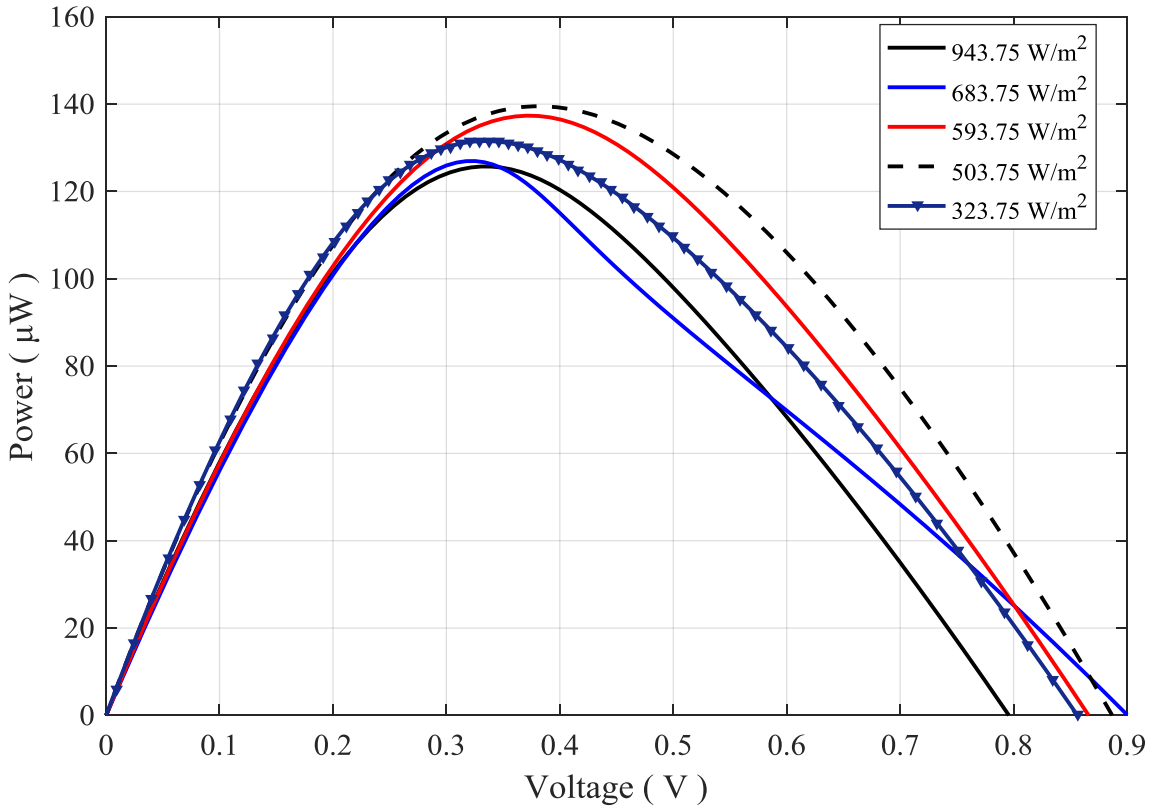

Fig. 3.8 Power characteristic curves of μ-PSCs under different irradiations for 2 days period (25 °C, pH 7).

3.3.3 pH effect on the power production

The effect of the pH on the power production from µ-PSCs is studied using the same technique developed for irradiation level study on µ-PSCs. Here, the optimal pH for the selected algae growth is pH 7 (*C. reinhardtii* CC-125). The generated power reduces when the pH of the anolyte solution is far from the optimal value. The result obtained and plot in *Fig. 3.9* shows the relation between the equation *(3. 5)* and the power generated by the µ-PSCs. Actually, the deviation of pH from the optimal growth pH increases the concentration of CO_2 in the anolyte. This situation affects the growth cycle of algae, therefore causing the reduction in the output power.

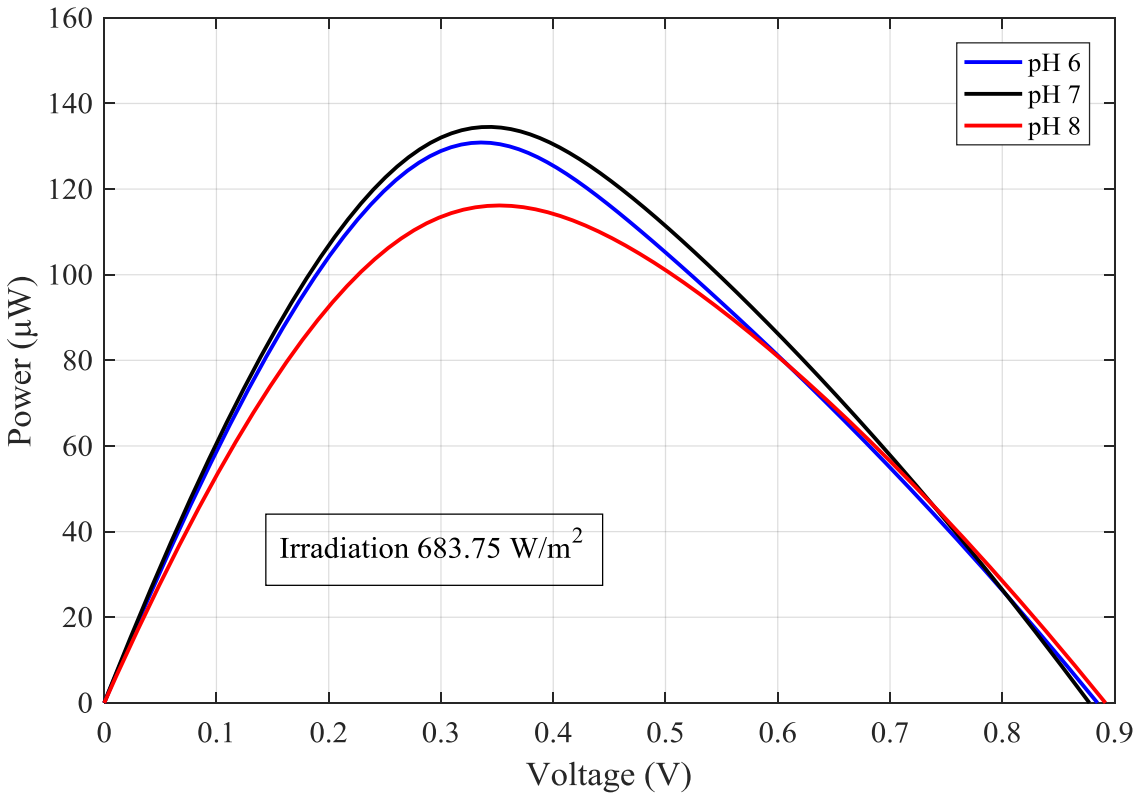

Fig. 3.9 Power characteristic curves of µ-PSCs for different anolyte pH (25 °C).

3.3.4 Effect of temperature on the power production

The pH of the solution in the anode chamber is found to have a significant impact on the output power compare to the effect of the temperature as one can see by comparing *Fig. 3.9* and *Fig. 3.10*. The *C. reinhardtii* CC-125 species optimal growing temperature is around 300 °K as proven in [13] and [28]. Therefore, we can say that small changes of the temperature around the optimal value has negligible effects. However, some practical tests should help find the temperature range for efficient power production from the cell. This can be done as a standalone study providing practical data from µ-PSCs.

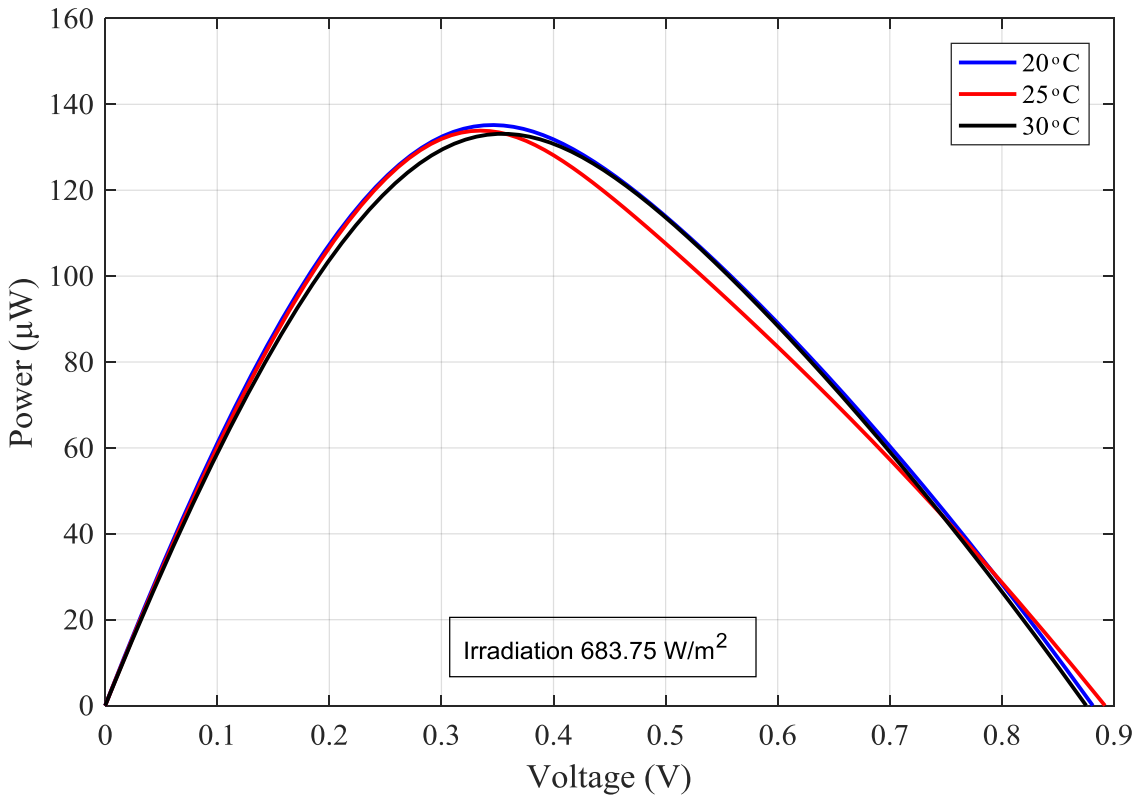

Fig. 3.10 µ -PSCs power characteristic curves under different temperature (pH 7).

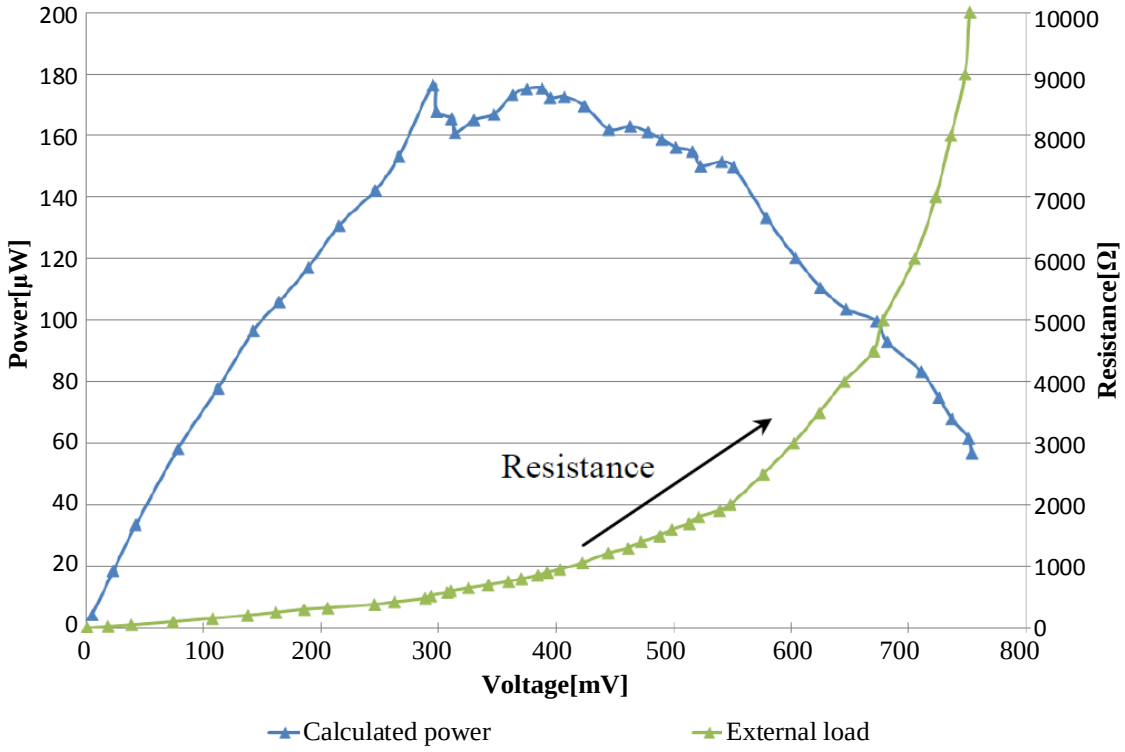

Fig. 3.11 Practical power characteristic curves of µ-PSCs [6].

One of the challenges faced by this technology is its applicability in real-world applications because of its actual low power output. In fact, despite the ongoing research advancement on µ-PSCs, the actual output power ability recorded is still in low hundreds of microwatts. The power monitoring circuits provided by many high tech companies generally operate at one power point. This in order to increase the efficiency of the harvesting circuits. The power monitoring circuits in [41] and [42] are some of the practical examples. Therefore, knowing the maximum operating point of the energy source, the main key to efficient use of such relatively efficient monitoring circuit (80% - 90%) is known.

3.3.5 Maximum power point location study

This work also focuses on finding theoretically, the range of voltage in which the maximum power point (MPP) occurs with μ-PSCs. Many simulations provided a range between 0.3V and 0.4V. Practical recorded data for a single cell (*Fig. 3.11*) and also results published by other works, such as in [6], [7], [19] and [28] on this topic showed the same result. Therefore, in terms of duty cycle, assuming that the open circuit voltage is between 0.953V and 0.991V; one can design a MPP tracker with duty cycle range between 0.303 and 0.420.

3.4 Conclusion

A dynamic electrochemical equivalent circuit for u-PSCs is developed and validated. Obtained results match well with the results from other sources related to photosynthetic power cells in terms of I-V and P-V curves. Also in terms of the temperature, the pH and the irradiation effects on the output of μ-PSCs. The developed model is general, it is a combination and conversion of the knowledge in biology and chemistry into electrical science. This model can therefore, be used to simulate any kind of photosynthetic power cell once the optimal living conditions required for the selected algae are known. Still, the model can be improved with results from practical experiments. However, this work should open the door to μ-PSCs simulation and emulation in order to reduce the costs related to trial and error methods and eliminate the time-consuming fabrication process. Furthermore, the knowledge of the maximum power point location should provide insights for the development and implementation of practical energy harvesting circuits for efficient power generation from this green technology.

Chapter 4: Energy harvesting circuit design

4.1 Introduction

Designing and manufacturing an energy harvesting circuit for low ultra-low energy sources (microamperes range) requires advanced technology especially during the manufacturing process. Practically, the power circuit topology is similar to a regular low power harvesting chargers like boost, buck, and buck-boost chargers. The challenge is in the manufacturing process of the components in order to obtain acceptable efficiency. The theoretical study of charging and energy harvesting circuits has been conducted in [43]. Different dc-dc converters for μ-PSC has been designed and evaluated using Matlab Simulink. Also, some of the maximum power tracking algorithms have been investigated. However, it seems impossible to practically implement the proposed harvesting charger circuit by using distinct elements as it is the case in regular chargers. This, because the current, and power levels under consideration are in micro level. Single chip charger circuits are solutions for such applications.

This chapter, instead of designing a boost charger, investigates the applicability of Integrated circuits (IC) with μ-PSCs by selecting one of the best energy harvesting ICs and studying its applicability with μ-PSCs. This chapter presents the advantages as well as the limitation of the IC BQ25504 [41] for energy harvesting and management. It also proposes an efficient energy harvesting method and circuitry using this IC for general low power energy sources and specifically for μ-PSCs. A circuit is prototyped and tested for proof of concept. This research work should open the door to the practical usage of μ-PSCs.

4.2 Design concept

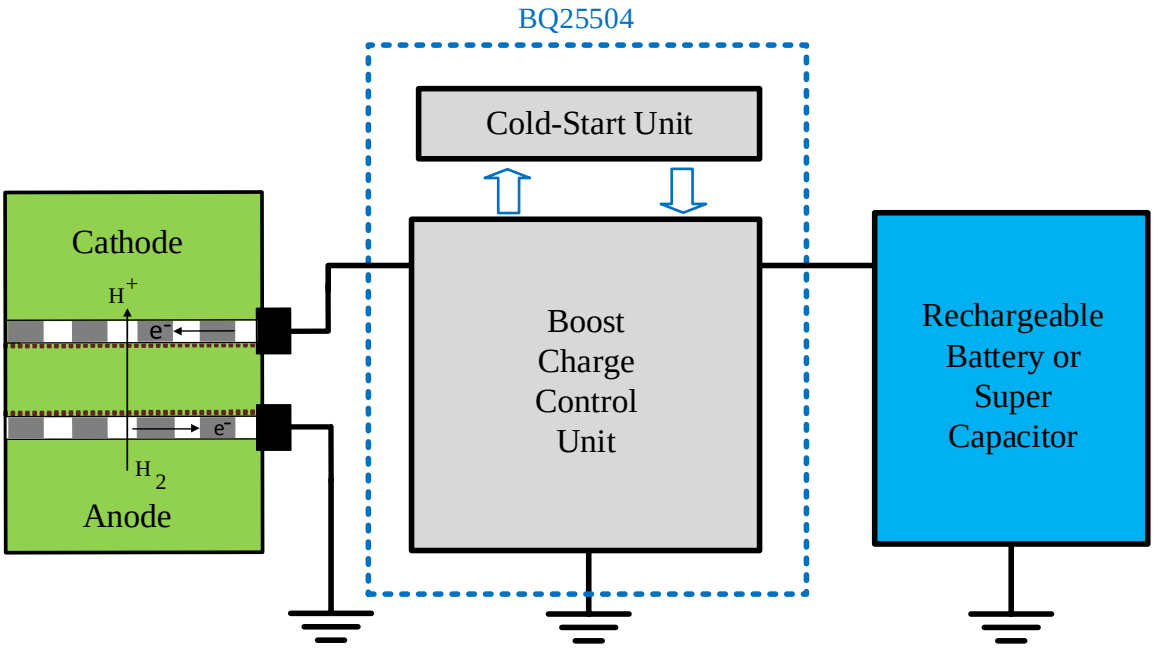

Fig. 4.1 General power monitoring configuration for μ-PSC.

The original block diagram of the energy harvesting circuit using the IC BQ25504 proposed by the manufacturer is shown in *Fig. 4.1*. The cold start unit is generally used to start the harvesting process automatically once a threshold voltage is reached. In other words, it triggers the boost charger operation.

The boost charger IC BQ25504 [41] is an ultra-low power boost converter with battery management and energy harvesting ability from Texas Instruments. It has a cold start voltage with input voltage regulation. The input voltage regulation prevents damage of the input source. The IC BQ25504 has energy harvesting capabilities for ultra-low power sources and can be used as solar chargers, thermal electric generator (TEG) harvesting, wireless sensor networks (WSNS), industrial monitoring, environmental monitoring,

bridge and structural health monitoring (SHM), smart building controls, portable and wearable health devices, and entertainment system remote controls [41].

The original design proposed by the manufacturer (*Fig. 4.2*) comprises many subunits which also includes an MPPT control unit. The programmable MPPT tracking embedded in the design has some limitations. In fact, in the MPPT method proposed, the MPPT point is calculated based on a fixed empirical value that should be specified by calculating the values of R_{CO1} and R_{CO2} during the design. The original design considers a constant ratio of the input voltage to be the MPPT operating voltage. The ratio is obtained via a simple voltage division of the input voltage using R_{CO1} and R_{CO2} and fed to the IC as the maximum point voltage.

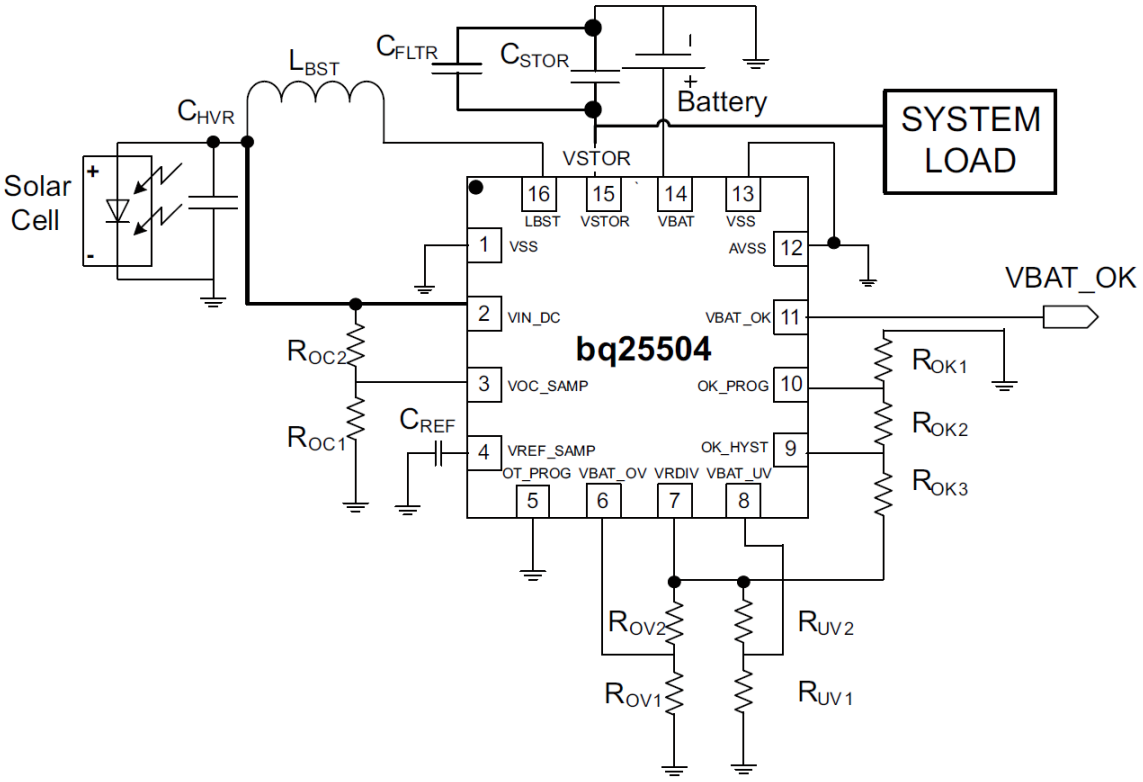

Fig. 4.2 Power monitoring configuration for the solar panel [41]**. Proposed by the manufacturer**

This technique is exceptionally useful for mature technologies such as the photovoltaics systems where the location of the MPPT can be estimated. Also, this design, by eliminating the MPPT scan, reduces the power consumption of the IC. Along with the power consumption reduction, this IC, thanks to its cold starting unit can start running with quite low voltages (330mV) and does not require external power. Its efficiency can be as high as 90%. However, despite the nice features depicted, the circuit in *Fig. 4.2* cannot be used for renewable energy source study except after some modifications.

The modifications consist of an external MPPT tracking unit for the dynamic maximum point tracking. This modification will help in the study the maximum power point of newly discovered/developed low energy sources on one hand. On the other hand, this unit can be used as a preliminary step for VOC_SAMP value determination for MPPT before calculating the values of R_{CO1} and R_{CO2}.

The updated desig*n in Fig. 4.3* includes the MPPT control unit. It is designed to facilitate the assessment of the power curves for low power sources. Knowing the power-voltage, current-voltage and power-current relationships can therefore, be investigated thanks to this integration. Once those three relations are known, one can extract the equivalent circuit for μ-PSCs and any low power energy source. The algorithm used for MPPT purposes is described in *Fig. 4.4*. The usage of this algorithm eliminates the need for R_{CO1} and R_{CO2} resistors. The output of the MPPT tracking unit is fed directly to $VREF\_SAMP$ on the IC trough C_{REF}.

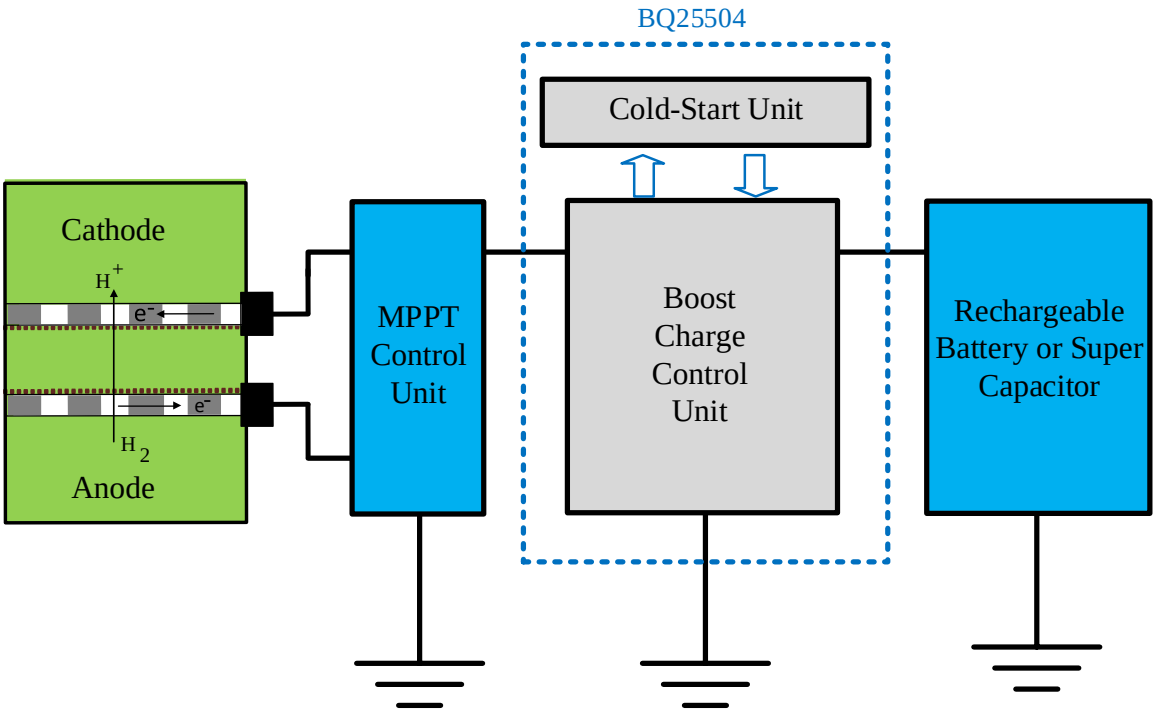

Fig. 4.3 Updated power monitoring configuration.

The dynamic output voltage and current of the μ-PSC are sensed using the sensing circuit developed in chapter 2. The corresponding maximum power point voltage is set based on the comparison of the actual sensed current and voltage values to the previously recorded samples. As can be seen from the flowchart, the algorithm is a modified hill-climbing algorithm. The value of $Vref$ ($VREF\_SAMP$) is set based on the calculated power level.

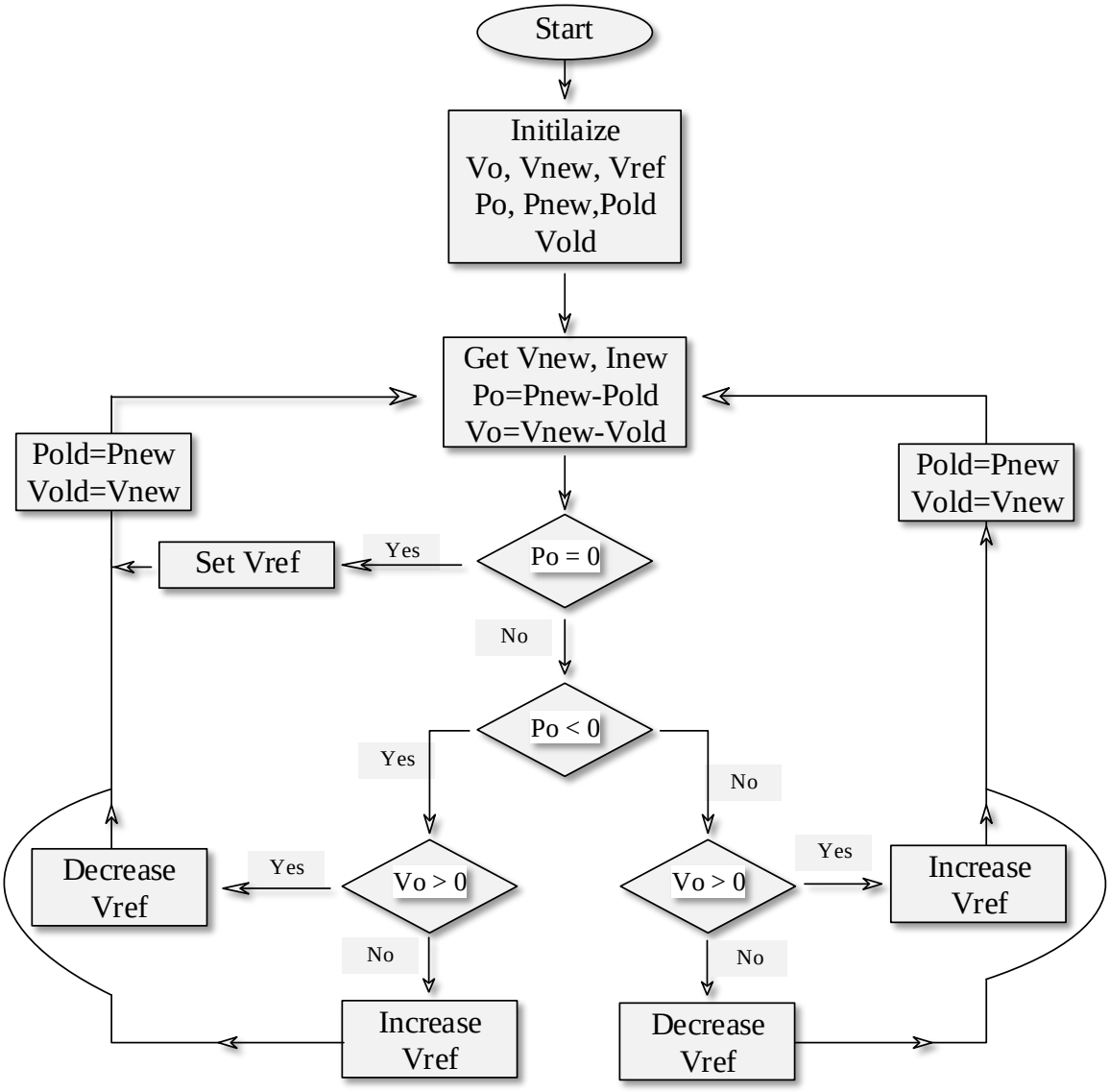

Fig. 4.4 Practical energy harvesting algorithm for the MPPT control unit.

The algorithm tracks the output power instantaneously and sets the reference voltage accordingly in order to always operate the circuit at the MPPT point. For a PV curve determination, one can directly vary the reference voltage from zero to the OC. This will automatically provide the I-V relationship thanks to the digital section of the sensing circuitry.

4.3 Hardware implementation

The hardware has all the constituents as described in *Fig. 4.3*. The MPPT control unit is formed by the current and voltage sensing circuitry and the MPPT tracking algorithm. The input probes are used to connect the input power source to the whole circuit. Current and voltage are monitored in order to run the MPPT algorithm. The output of the algorithm known as $Vref$ is sent to the harvesting unit in the form of an analog signal. The setting of $Vref$ enables the boost charger to run the at the MPPT point. Finally the load is fed by a 2.5 to 5 V dc source thanks to the improved boost ability of the selected boost charger.

All the parameters on *Fig. 4.2* are calculated based on the datasheet provided by the manufacturer. The design specifications for the solar panel is listed in *Table 4.1*.

Table 4. 1 Design specifications of the energy harvesting IC for solar panel

Solar Panel	***Description***	***Design value***
VBAT_OV	Maximum comparator voltage (Typically maximum battery voltage)	5.2V Ni-MH battery
VBAT_OK_HYST	Maximum comparator threshold voltage	5 V
VBAT_OK	Nominal Voltage of the Battery	4.8 V
VBAT_UV	Minimum comparator threshold voltage	4V
VREF_SAMP	Maximum power point threshold	0.8V With VIN_DC(OC)= 2.5 V

Table 4. 2 Design parameters of the energy harvesting IC for solar panel

	Description	***Calculated value***
C_{HVR}	Input capacitance	4.7 μF
L_{BST}	Input inductance	22 μH
R_{OC1}	Resistance for setting the MPPT reference.	6.34 ±1% MΩ
R_{OC2}	Resistance for setting the MPPT reference.	3.57 ±1% MΩ
R_{OV1}	Resistance for setting reference over-voltage.	3.57 ±1% MΩ
R_{OV2}	Resistance for setting reference over-voltage.	6.34 ±1% MΩ
R_{UV1}	Resistance for setting reference under-voltage.	3.4 ±1% MΩ
R_{UV2}	Resistance for setting reference under-voltage.	6.49 ±1% MΩ
R_{OK1}	Resistance for setting reference voltage.	3.24 ±1% MΩ
R_{OK2}	Resistance for setting reference voltage.	6.04 ±1% MΩ
R_{OK3}	Resistance for setting reference voltage.	0.523 ±1% MΩ
C_{REF}	Sampled reference storage capacitance	10 pF
C_{STOR}	Storage capacitance	4.7 μF
CBAT	Battery pin capacitance or equivalent battery capacity	100 μF

Ni-MH Batteries rated 1.2 V, 500mAH were used in series as the load. The output of the boost charger is set to 4.8V for the tested solar panel because of its relatively high OCV (4.5V under 800w/m2 irradiation level) and MPPT points (0.8xVoc).

For the micro-photosynthetic cell, the OCV is near 1V and has a variable MPPT as described in chapter 3. The design specifications are listed in *Table 4.3*. 3.6 V is set as the output voltage of the boost charger.

Table 4.3 Design specifications of the energy harvesting IC for µ-PSCs

µ-PSCs	***Description***	***Design value***
VBAT_OV	Maximum comparator voltage (Typically maximum battery voltage)	4V Ni-MH battery
VBAT_OK_HYST	Maximum comparator threshold voltage	3.8 V
VBAT_OK	Nominal Voltage of the Battery	3.6 V
VBAT_UV	Minimum comparator threshold voltage	3.0 V
VREF_SAMP	Maximum power point threshold	0.38 V With VIN_DC(OC)= 0.9 V

Table 4.4 Design parameters of the energy harvesting IC for µ-PSCs

	Description	***Calculated value***
C_{HVR}	Input capacitance	4.7 µF
L_{BST}	Input inductance	22 µH
R_{OC1}	Resistance for setting for MPPT reference.	8.45 ±1% MΩ
R_{OC2}	Resistance for setting for MPPT reference.	1.58 ±1% MΩ
R_{OV1}	Resistance for setting reference over-voltage.	4.64 ±1% MΩ
R_{OV2}	Resistance for setting reference over-voltage.	5.23 ±1% MΩ
R_{UV1}	Resistance for setting reference under-voltage.	4.12 ±1% MΩ
R_{UV2}	Resistance for setting reference under-voltage.	5.76 ±1% MΩ
R_{OK1}	Resistance for setting reference voltage.	3.24 ±1% MΩ

	Description	***Calculated value***
ROK2	Resistance for setting reference voltage.	6.04 ±1% MΩ
ROK3	Resistance for setting reference voltage.	0.523 ±1% MΩ
CREF	Sampled reference storage capacitance	10 pF
CSTOR	Storage capacitance	4.7 µF
CBAT	Battery pin capacitance or equivalent battery capacity	100 µF

Based on the design parameters obtained, four circuits were prototyped for solar panel and µ-PSCs each of them having two designs. One circuit with the straightforward operation design as proposed by the manufacturer and another one with external MPPT circuit for MPPT improvement. The final design combined the straightforward design and the updated design using an external switch. The figure below shows the MPPT charger prototype.

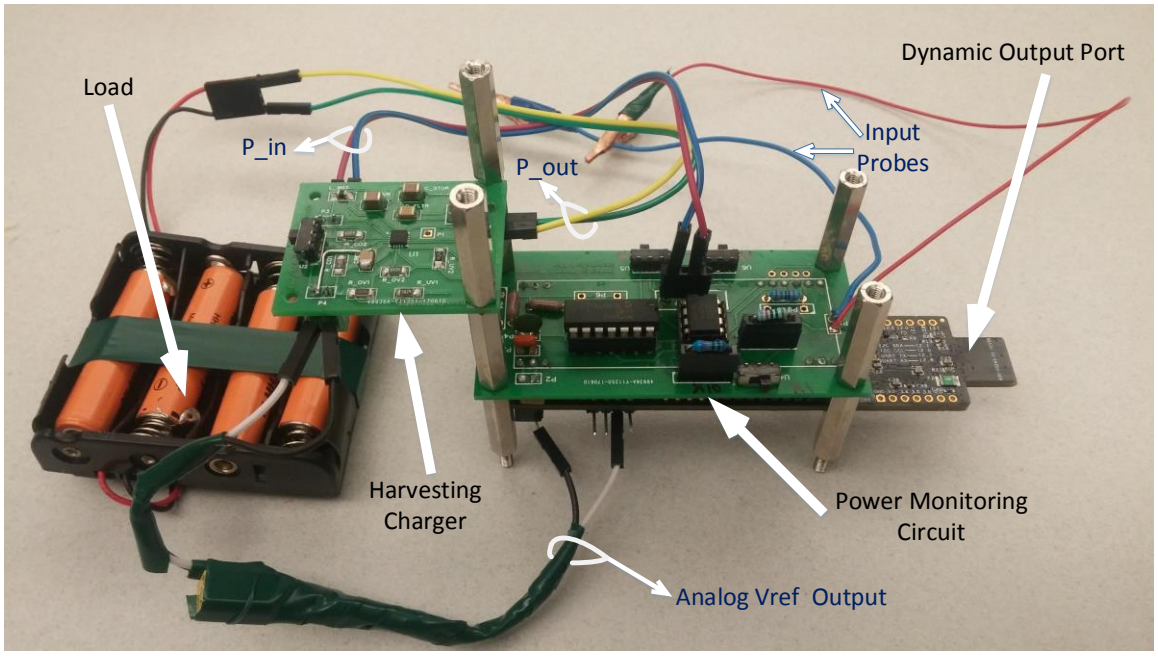

Fig. 4.5 Harvesting circuit prototype.

The block diagram below shows in detail the electrical configuration and the operation mechanism of the MPPT charging circuit.

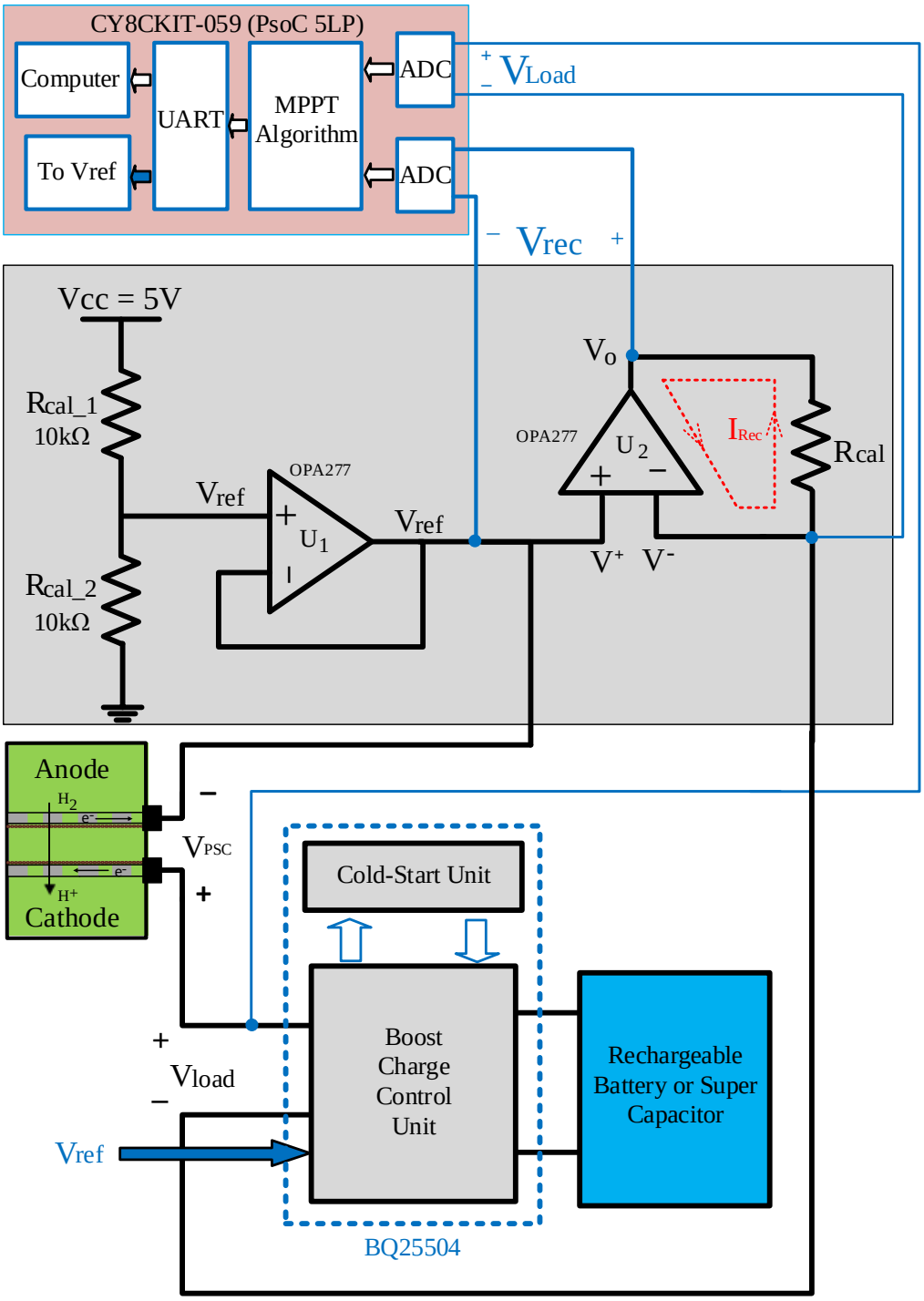

Fig. 4.6 Schematic layout of the harvesting circuit.

The output provided by the UART port enables the visualization of the performance of the whole unit by recording and displaying the current and voltage values at any operation point from the power input side. For most of the tests, the solar panel in the figure below is used. The algae cultivation process along with the practical inherent problems related to μ-PSCs such as film formation on the surface of the anode surface limits the availability of the μ-PSCs for every single test.

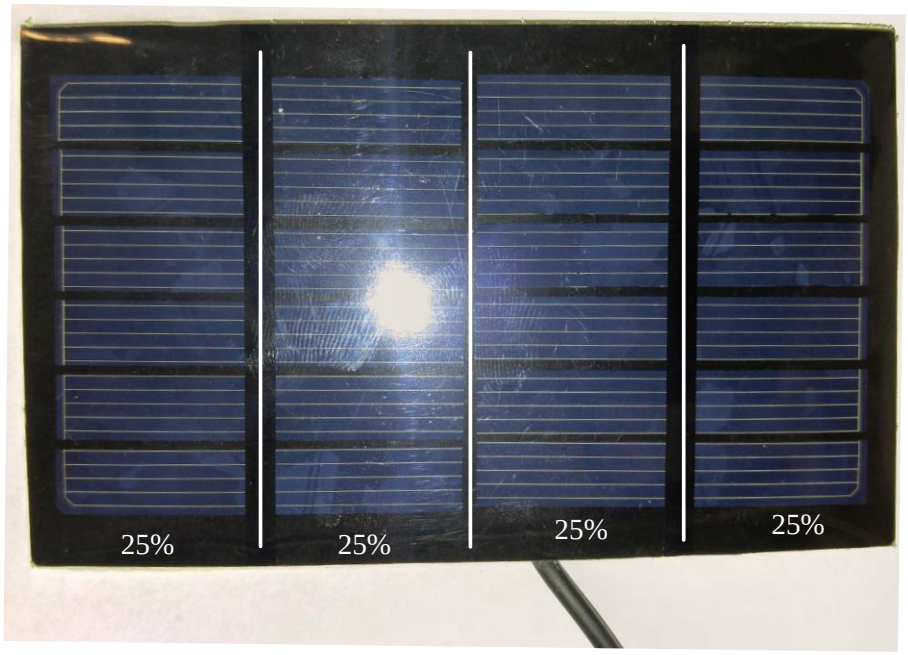

Fig. 4.7 Solar panel for the MPPT test.

The unit subdivision of this solar panel allows easy illumination level variations in order to induce a step change in the input power. This step change will enable the validation of the dynamic behavior of the improved design over the proposed design by the manufacturer (original design).

The testing setups for the dynamic MPPT test, the charging ability test and the efficiency of the harvester study are shown in the following figures.

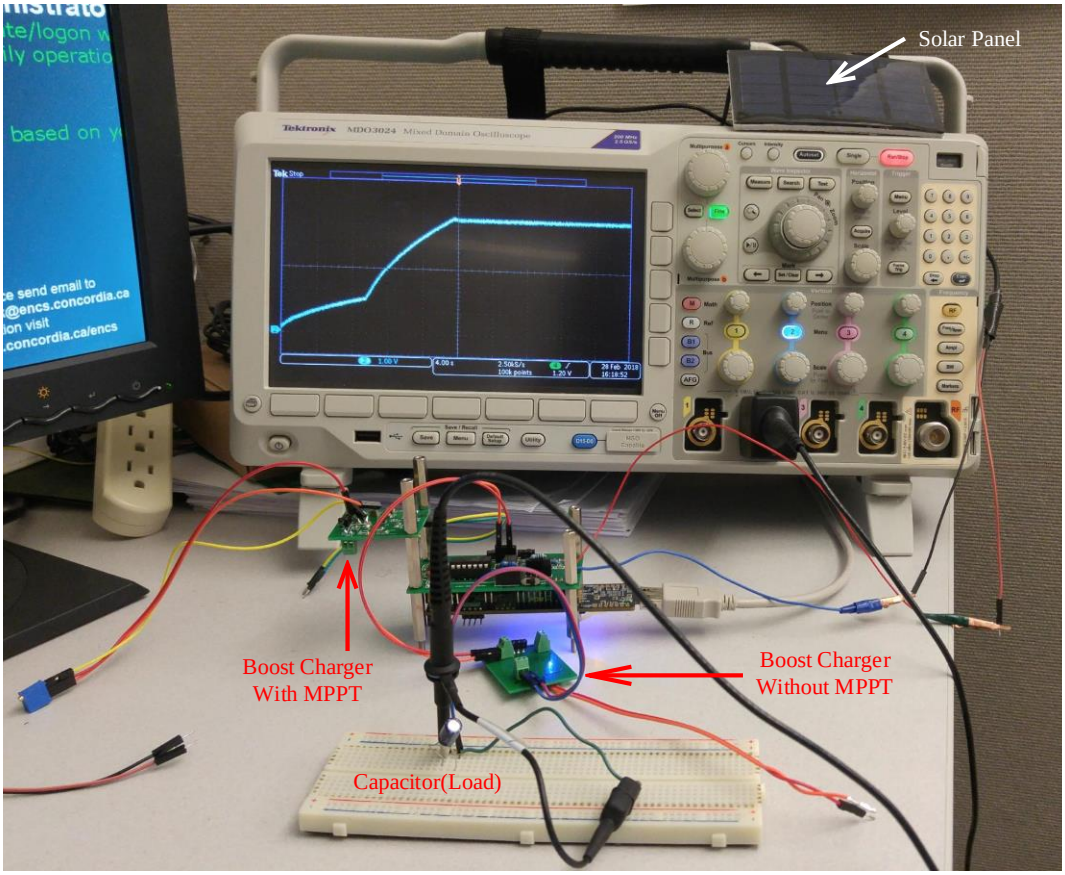

Fig. 4.8 Experimental setup with a photovoltaic cell

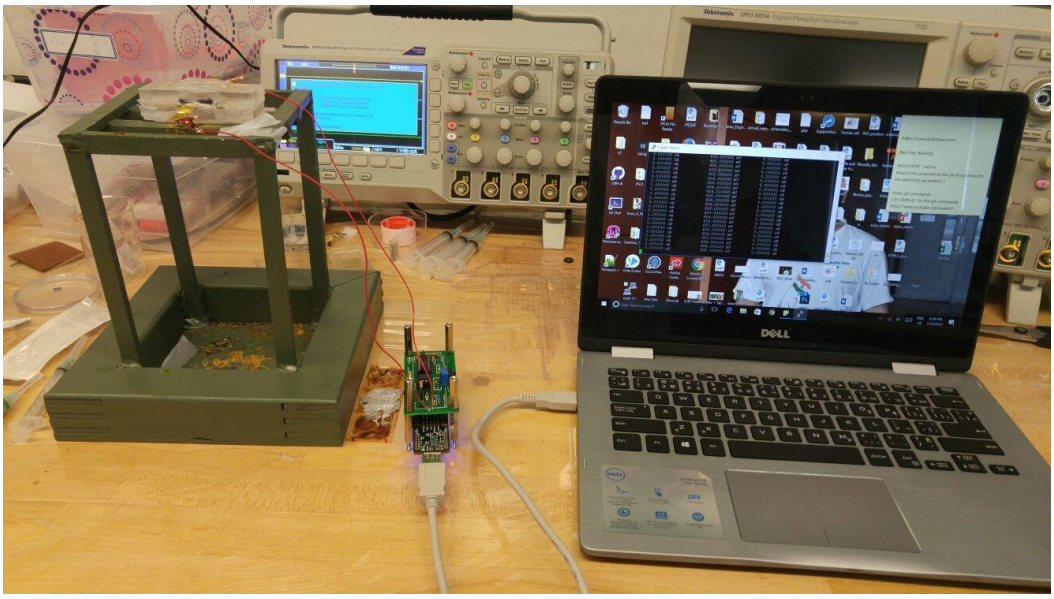

Fig. 4.9 Experimental setup with the µ-PSC.

4.4 Results

4.4.1 MPPT tracking (with straightforward design)

The dynamic MPPT test is performed using the solar panel to serve as the worst case scenario. In fact because of the electrochemical reactions occurring the μ-PSCs, and also as proven in chapter 3, the dynamics in the μ-PSCs are much slower compared with those in solar cells. The irradiance-output power relationship of solar cells is predictable and well known. We found the solar cell more suitable for dynamic testing of the MPPT tracking ability of the circuit.

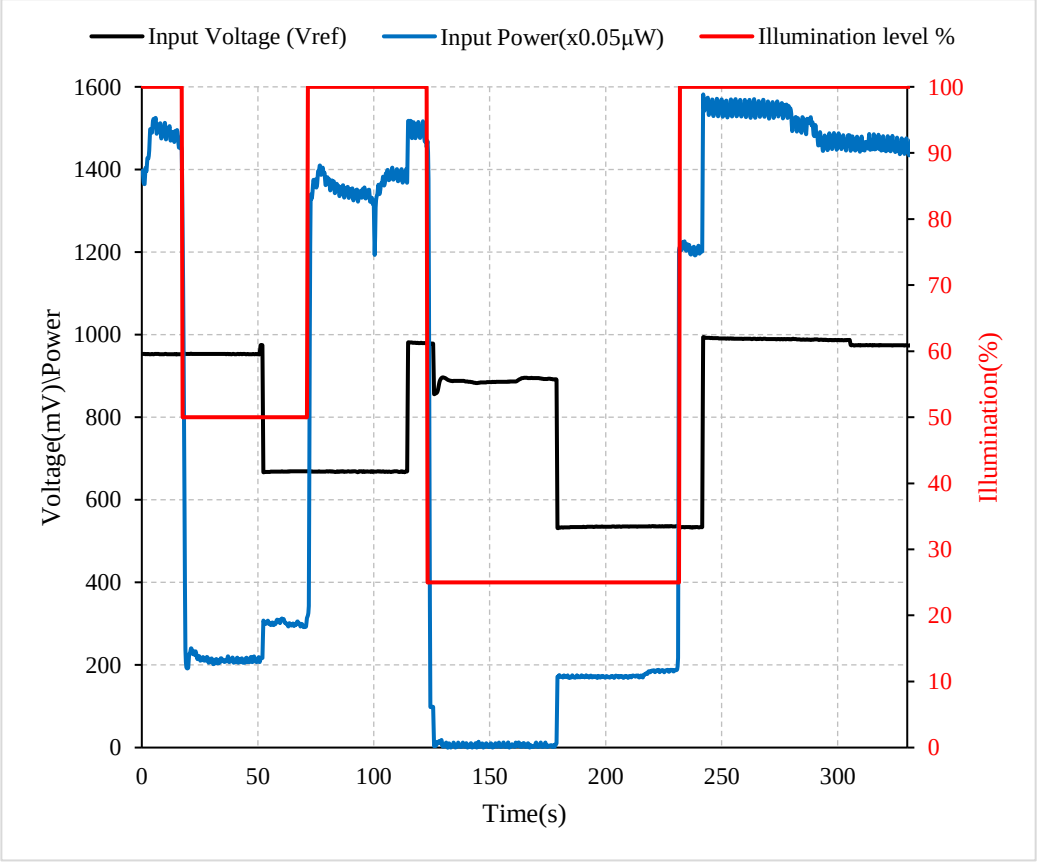

Fig. 4.10 Instantaneous power tracking without MPPT circuit: Power-Voltage relationship.

For this experiment, a step change in the incident light intensity on the solar panel was used to emulate the worst case scenario. The illumination in the laboratory was the main source of light. During the experiment, the solar panel was covered in 0%, 50%, 0%, 75%, 0% sequence to simulate the step change in the irradiance. The design in *Table 4. 2* is used to implement the harvesting circuit. As depicted in *Fig. 4.10*, during the 0% to 50% illumination reduction, it took almost 30 seconds for the original design to adjust the solar panel's terminal voltage for maximum power output. During the step reduction of illumination from 0% to 75%, the time required to operate at MPPT is almost doubled leading to a zero power output from the solar panel during that interval of time. The observations also show that there is always a delay before the operation of MPPT circuit in the original design. This delay occurs during step change in both directions (increasing and decreasing illumination levels). This, unfortunately, causes the power loss and therefore, this design is not suitable for high dynamics micro level power sources.

The voltage and current curves obtained with the original design during the step change in the illumination are shown in *Fig. 4.11*. The change in the input voltage is not smooth. This proves the nonexistence of the maximum power point searching logic in the design, or the existing MPPT logic is poorly designed.

The current waveform is normal in the sense that it is related to the illumination level on one hand. On the other hand, the boost charger tries to keep the voltage at the battery terminal constant. Therefore it controls the input voltage to the IC in order to provide the maximum current possible for the battery charge.

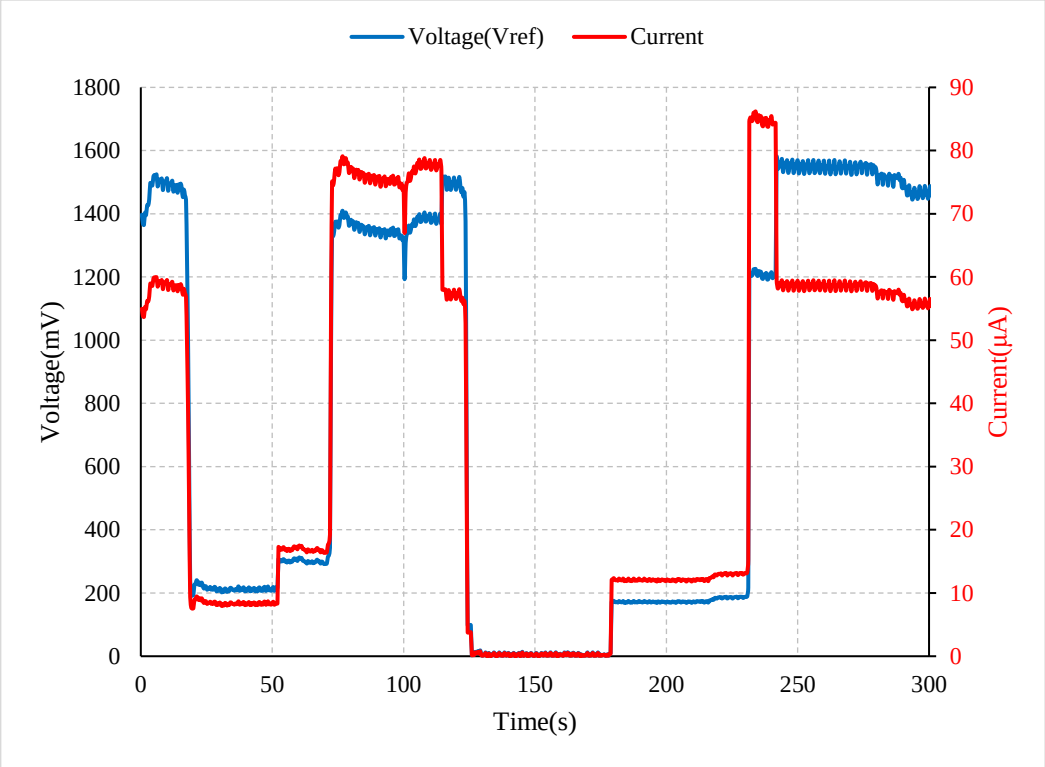

Fig. 4.11 Instantaneous power tracking without MPPT circuit: Voltage-Current waveforms.

4.4.2 Dynamic MPPT tracking test (with the MPPT block)

For this experiment, the testing procedure and the sequence in the illumination are unchanged. Only the experimental setup is changed by activating the external MPPT circuit. As depicted in *Fig. 4.12*, the output power from the cell is directly related to the irradiation level unlike the result obtained in *Fig. 4.10*. However, the change in the output voltage varies in the direction of the maximum power point location. It has a smooth change and one can see that even at maximum power point the algorithm tries to find a possible global maximum power point. The output current is mostly influenced by the irradiation level and follows almost the same pattern as the output power. The input voltage to the harvesting IC operates as a controller of the input current to the harvesting IC for maximum power operation (*Fig. 4.13*).

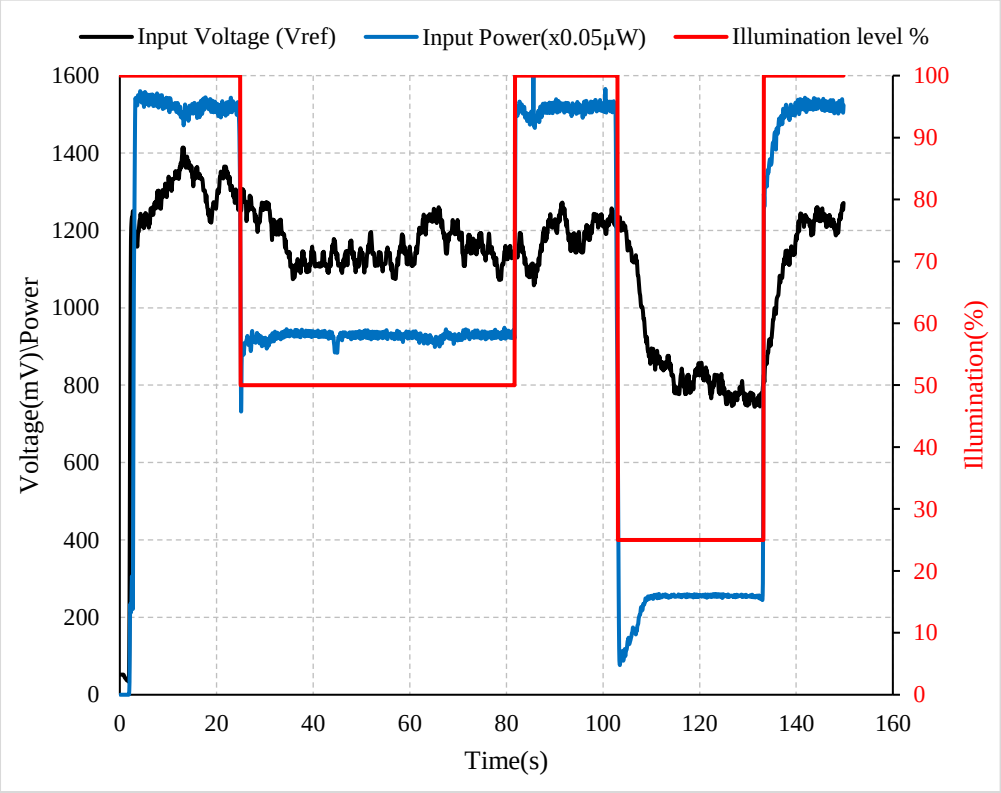

Fig. 4.12 Instantaneous power tracking with MPPT circuit: Power-Voltage relationship.

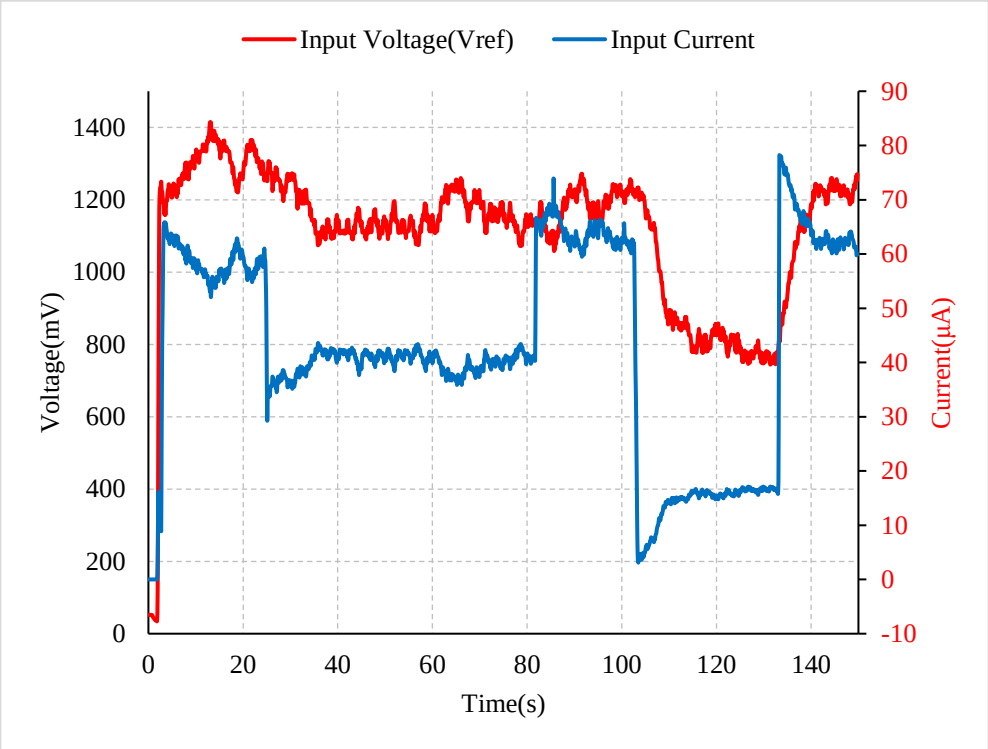

Fig. 4.13 Instantaneous power tracking with MPPT circuit: Voltage-Current waveforms.

The ability of the developed circuit to operate with higher dynamics by keeping in track the MPPT for instantaneous maximum power output proves its ability to smoothly operate with μ-PSCs. Also, this proves that this circuit can be used in the study of the micro level power sources that have similar or slower dynamics compared to solar cells. Unfortunately, no working μ-PSC was available for test after prototyping this harvesting circuit. However, based on the observations with the solar panel, one can deduce the ability of this circuit to work with the μ-PSCs.

4.4.3 Charging test

The setup in *Fig. 4.8*, is used to verify the charging ability of the boost charger. The setup consists of a solar panel, the MPPT circuit, the boost charging IC and the oscilloscope. The battery bank available is rated 500mAH. It will take "an eternity" to fully charge with the average 12μA current available from the solar panel. In order to get and validate the charging curve, a 33 μF capacitor is used instead of the battery bank. With this configuration, the capacitor is expected to be fully charged in approximately 13.75 seconds from zero to 5.2V (VBAT_OV). The oscilloscope used is set to a small time scale to enable the full display of the waveform. *Fig. 4.14* shows the charging curve of the battery (capacitor). The capacitor was initially short-circuited in order to discharge it completely before the charging test. Also before the experiment, the solar panel was totally covered in order to disable the main boost charger in the IC and also the cold starting unit. Recalling that below 300mV the IC is completely disabled.

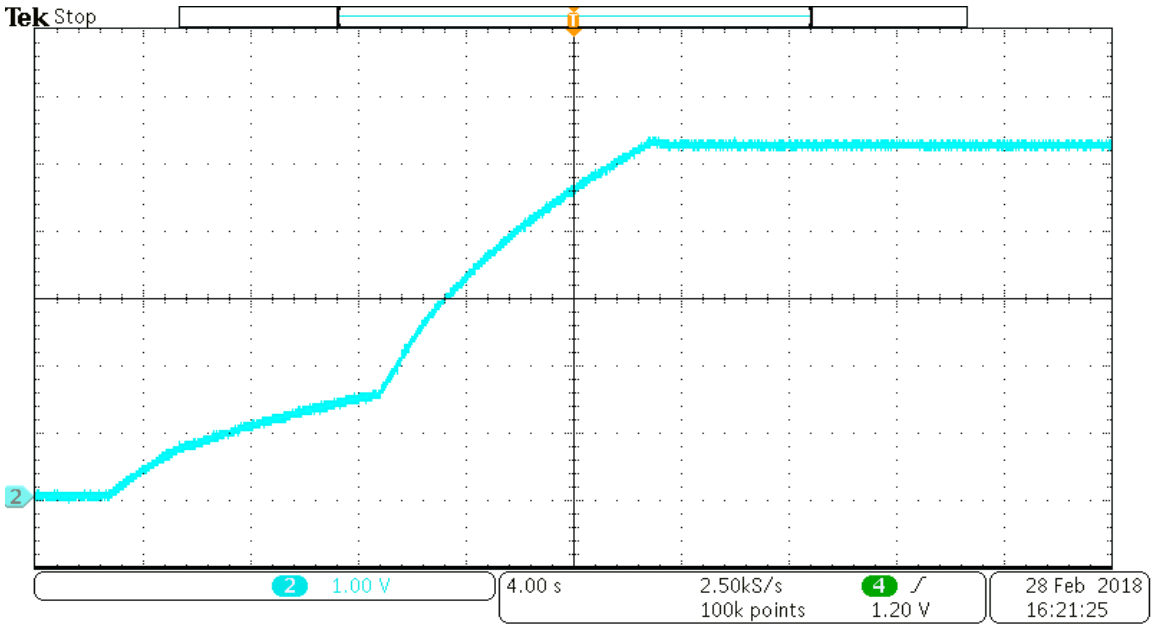

Fig. 4.14 Charger operation after a depleted storage element is attached and harvester is available.

The study of the charging curve based on our design requirements as specified in *Table 4. 1*, provided the information as summarized in the *Fig. 4.15*. The device functional modes are depicted through this test.

The result shows that the output of the boost charging IC is 0V when the input voltage to the IC is less than 300mA. This is expected from the datasheet point of operation of the IC. The operation of the cold starting unit started just after we began uncovering the solar panel. The operation of the cold starting circuit charged the capacitor up to VSTOR_CHGEN before the boost charger begun the operation. During the boost charger operation, the capacitor voltage reached the VBAT_OV which is the maximum voltage allowed by the battery as per the design in *Table 4. 1.* VBAT_OV is also the maximum output voltage of the boost charger per the design. Once the battery is fully charged, the IC sets the maximum power point to the open circuit. Therefore, no power is drawn from

the source. Practically, a load will be connected to the terminal of the battery. In this case, the IC instead of stopping its operation will supply the load by making sure that the battery remains fully charged. Therefore, some ripples may be observed at VBAT_OV depending on the load used and its loading cycles.

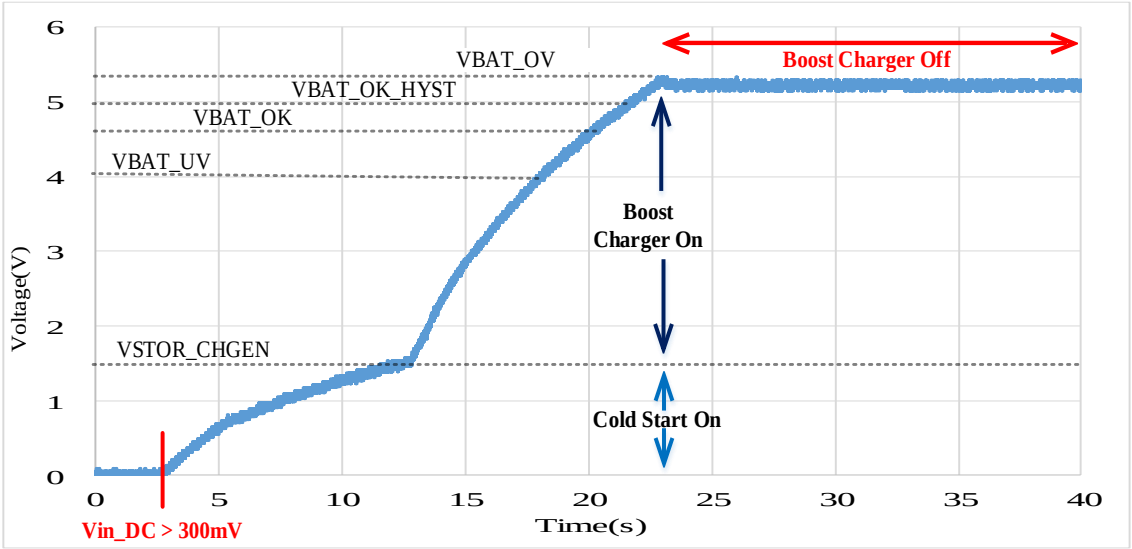

Fig. 4.15 Device functional modes.

4.4.4 Efficiency study

This efficiency study is solely for the energy harvesting circuit. The power consumed by the dynamic MPPT tracking unit is not included in the efficiency calculation. The reason is that practically the MPPT unit is required at the beginning of the design process in order to identify the average MPPT point. Once this information is known, the reference voltage can be set using R_{CO1} and R_{CO2} even though this method is not too efficient.

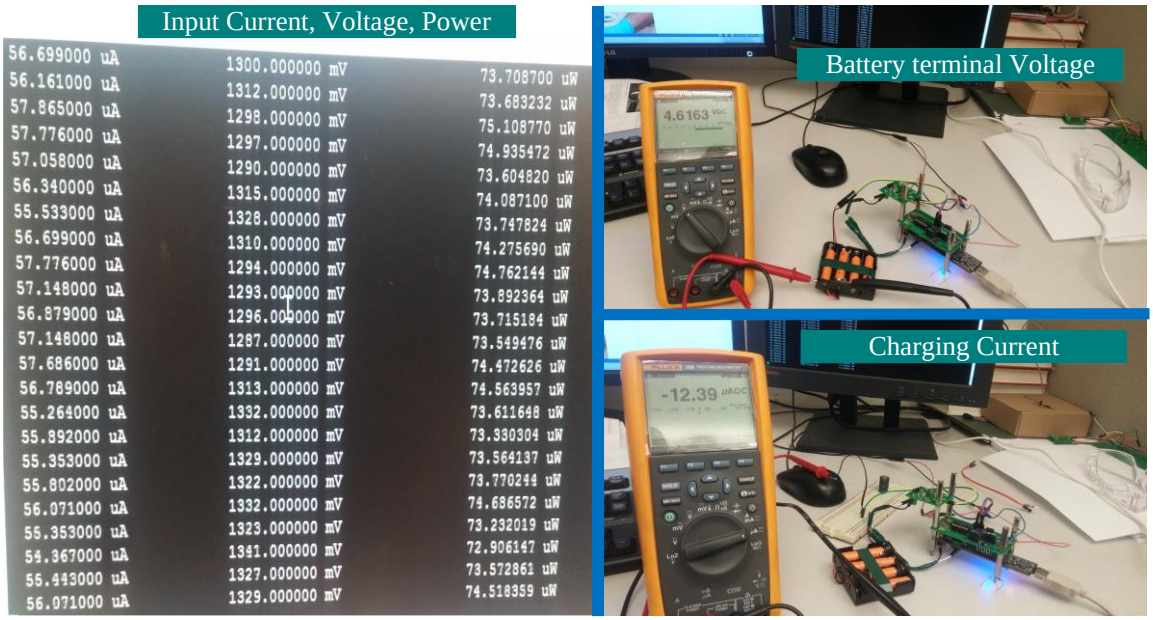

Fig. 4.16 Practical data for efficiency calculation for the power harvesting circuit.

Table 4.5 Energy Harvesting Efficiency

Measured	***Description***	***Value***
$P_{in_{avg}}$	Average input power	3.96 µW
$Vout$	Recorded battery terminal voltage	4.6163 V
$Iout$	Recorded charging current	12.39 µA
Efficiency	Efficiency of the energy harvester	77.33%

The efficiency is quite acceptable considering the boost charger manufacturer's datasheet. The boost charger does not require external power for its operation. In this case, almost 22.67% percent of the energy provided by the low power source is consumed during the IC operation.

4.5 Conclusion

This chapter focused on the testing and upgrading the existing technology related to the energy harvesting of low power energy sources such as μ-PSCs. Although the tests are performed using a low power rated solar panel, the results showed that the updated boost charging IC empowered with the MPPT tracking algorithm can be used for energy studies of very low energy sources. Testing μPSCs with this circuitry as a future work should provide better and accurate characterization curves knowing that the best way of getting the characteristic curves especially for renewable energy sources is the use of dc converters for operating point scans instead of resistive load.

Chapter 5: Conclusions and future work

5.1 Conclusions

This research work focused on monitoring the energy from very low power sources and especially from μ-PSCs. The research provided a real-time current sensing circuit designed, prototyped and tested for use in the characterization and the power monitoring of μ-PSCs. Obtained readings are dynamic and with acceptable accuracy up to the second digit in a range starting from nA to a few mA thanks to the calibration process developed in the digital environment. The prototyped circuit is used to record dynamic data from the μ-PSC and was able to cover the full power range without loss in accuracy. The data obtained are used in the validation of the electrochemical model developed to emulate the μ-PSCs.

The electrochemical modeling of μ-PSCs presented in chapter 3 is based on the research outputs from different works on green algae's photo-respiration mechanism on the one hand and on the second hand, on the experimental results. The model results match with the results from other sources related to photosynthetic power cells in terms of the I-V and P-V curves, the temperature, the pH, and irradiation effects on the output power. The developed model is general. It is a combination and conversion of knowledge in biology, and chemistry into electrical science. This model can therefore, be used to simulate any kind of photosynthetic power cell once the optimal living conditions required for the selected algae are known. Still, the model can be improved with results from practical experiments. However, this work should open the door to micro photosynthetic power cell simulation and emulation area in order to reduce the cost related to trial and error methods and eliminate the time-consuming fabrication process. Furthermore, the

knowledge of the maximum power point location provided insights for the development and implementation of practical energy harvesting circuits as presented in chapter 4.

In chapter 4, we come up with a circuitry that is able to characterize and harvest energy from low power sources with acceptable efficiency. The circuit is the upgrade of one of the existing technologies developed for the energy harvesting from low power energy sources. Most of the tests are performed using a low power rated solar panel for worst case scenario analysis. The results of this analysis showed that the updated boost charging IC empowered with the MPPT tracking algorithm can be used for energy studies of very low energy sources and also can increase the dynamic power harvested by the IC.

5.2 Future work

The process involved in the fabrication process of the μ-PSC requires more attention and time. Not only the algae should be cultivated before the test, but also they should be maintained alive at the appropriate living conditions (pH, temperature, illumination, day & night cycles etc.) and also by supplying them with nutrients (carbon dioxide, oxygen, nitrogen, and phosphorus). The electrical parts regarding monitoring and harvesting circuitry although they were great challenges; designing, prototyping, testing and calibrating them provided an easy way for a rapid test of μ-PSCs. This will enable a fast data collection and therefore minimize the overall cost and time in the fabrication and testing process of the μ-PSCs that will be fabricated in future. Future work includes,

- The dynamic data output ability of the sensing circuit should be able to facilitate μ-PSC testing and provide a better understanding of the dynamics involved in the power generation form μ-PSC.

- The effect of each parameter on the photosynthesis and electrons liberation in the reaction chamber should be investigated using the real-time monitoring circuit in order to improve the cell fabrication and also of the electromechanical model of μ-PSCs.
- The developed model should be improved with results from practical experiments to test its applicability.
- This work by opening the door to the micro photosynthetic power cell simulation area should be used as a prior step before any fabrication process of the μ-PSC in order to reduce the cost related to trial and error methods and eliminate the time-consuming fabrication process.
- Furthermore, the knowledge of the maximum power point location should provide insights for the development and implementation of more efficient energy harvesting circuits for power monitoring from this green technology.
- Testing μPSCs with the developed circuitry as a future work should provide better and accurate characterization curves knowing that the best way of getting the characteristic curves especially for renewable energy sources is the usage of dc converters for smooth operating points scan instead of resistive loads.

References

[1] K. B. Lam, M. Chiao and L. Lin, "A micro photosynthetic electrochemical cell," in *Micro Electro Mechanical Systems, 2003. MEMS-03 Kyoto. IEEE The Sixteenth Annual International Conference on*, Kyoto, Japan, 2003.

[2] K. T. Hemanth, S. M. Resmi, V. R. Aravind, M. Shahparnia, P. Muthukumaran, P. Pragasen, W. Sheldon, J. Philippe and R. Raghunathan, "Micro photosynthetic cell for power generation from algae: Bio-electrochemical modeling and verification," *J. Technology,* vol. 4, no. 4, pp. 249-258, 2016.

[3] P. Cristian, P. K. Krishna, C. M. V. L. Mark, M. H. Ian and S. Keith, "Modelling microbial fuel cells with suspended cells and added electron transfer mediator," *J Appl Electrochem,* vol. 40, p. 151–162, 2010.

[4] C. Siu and M. Chiao, "A Microfabricated PDMS Microbial Fuel Cell," *J. Power Sources,* vol. 152, pp. 175-181, 2005.

[5] C. P. B. Siu and M. Chiao, "A Microfabricated PDMS Microbial Fuel Cell," *J. Microelectromechanical Systems,* vol. 17, no. 6, pp. 1329-1341, December,2008.

[6] M. Shahparnia, "Polymer Micro Photosynthetic Power Cell: Design, Fabrication, Parametric Study and Testing," M.A.Sc. thesis, Dept., Mech. Eng., Concordia Univ., Montreal, QC, 2011.

[7] A. V. Ramanan, M. Pakirisamy and S. S. Williamson, "Advanced Fabrication, Modeling, and Testing of a Microphotosynthetic Electrochemical Cell for Energy Harvesting Applications," *IEEE Trans. Power Electronics,* vol. 30, no. 3, pp. 1275 - 1285, 2015.

[8] Y. Satake, Y. Otani and I. Maeda, "Photosynthetic fuel cell using purple non-sulfur bacteria," in *Optomechatronic Technologies (ISOT), 2012 International Symposium on*, Paris, France , 2012 .

[9] M. Ma, X. Shi, L. Cao and Z. Deng, "The operation of photosynthetic microbial fuel cells powered by Anabaena variabilis," in *Materials for Renewable Energy and Environment (ICMREE), 2013 International Conference on*, Chengdu, China , 2014.

[10] J.-G. Ha, S.-K. Lee, S.-J. Bai, Y.-S. Song, Y.-K. Kim, Y.-M. Shin and J.-H. Park, "Implementation of stackable photosynthetic microbial fuel cell structure using stainless steel mesh membrane electrode assembly," in *Solid-State Sensors,*

Actuators and Microsystems (TRANSDUCERS), 2015 Transducers - 2015 18th International Conference on, Anchorage, AK, USA , 2015.

[11] M. Guarnieri, V. D. Noto and F. Moro, "A Dynamic Circuit Model of a Small Direct Methanol Fuel Cell for Portable Electronic Devices," *IEEE Transactions on Industrial Electronics*, vol. 57, no. 6, pp. 1865 - 1873, 2010.

[12] R. P. Pinto, B. Srinivasan and B. Tartakovsky, "A unified model for electricity and hydrogen production in microbial electrochemical cells," in *18th IFAC World Congress (IFAC'11)*, Milano (Italy), 2011.

[13] H. Lee and S. Choi, "A micro-sized bio-solar cell for self-sustaining power generation," *Lab Chip*, vol. 15, no. 2, p. 391–398, 2015.

[14] X.-C. Zhang and A. Halme, "Modelling of a microbial fuel cell process," *Biotechnology Lett.*, vol. 17, no. 8, pp. 809-814, 1995.

[15] M. Chiao, K. B. Lam and L. Lin, "Micromachined microbial and photosynthetic fuel cells," *J. Micromech. Microeng*, vol. 16, no. 12, pp. 2547-2553, 2006.

[16] S. C. JAMES and V. BORIAH, "Modeling Algae Growth in an Open-Channel Raceway," *J. Computational Biology*, vol. 17, no. 7, p. 895–906, 2010.

[17] A. Thornton, T. Weinhart, O. Bokhove, B. Zhang, D. v. d. Sar, K. Kumar, M. Pisarenco, M. Rudnaya, V. Savcenco, J. Rademacher, J. Zijlstra, A. Szabelska, J. Zyprych, M. v. d. Schans, V. Timperio and F. Veerman, "Modeling and optimization of algae growth," CASA-Report 10-59, Eindhoven (Netherlands), 2010.

[18] S. K. Jayaraman and R. R. Rhinehart, "Modeling and Optimization of Algae Growth," *Ind. Eng. Chem. Res*, vol. 54, no. 33, p. 8063–8071, 2015.

[19] C. Picioreanu, K. Katuri, M. Van Loosdrecht, I. Head and K. Scott, "Modelling microbial fuel cells with suspended cells and added electron transfer mediator," *J. Appl. Electrochem.*, vol. 40, p. 151–162, 2010.

[20] W. J. Henley, "Measurement and interpretation of photosynthetic light-response curves in algae in the context of photoinhibition and diel changes," *J. Phycol.*, vol. 29, no. 6, pp. 729-739, 1993.

[21] M. Vítová, K. Bišová, D. Umysová, M. Hlavová, S. Kawano, V. Zachleder and M. Cížková, "Chlamydomonas reinhardtii: duration of its cell cycle and phases at growth rates affected by light intensity," *Planta,* vol. 233, pp. 75-86, 2011.

[22] B. Quentin, S. Andy and G. Benoit, "Modeling the effects of light and temperature on algae growth: State of the art and critical assessment for productivity prediction during outdoor cultivation," *Biotechnol. Adv.*, vol. 31, no. 8, pp. 1648-1663, 2013.

[23] V. Milada, B. Kateřina, H. Monika, K. Shigeyuki, Z. Vilém and Č. Mária, "Chlamydomonas reinhardtii: duration of its cell cycle and phases at growth rates affected by temperature," *Planta,* vol. 234, no. 3, pp. 599-608, 2011.

[24] J. P. Decker, "Effect of temperature on photosynthesis and respiration in red and loblolly pines," *Plant Physiology,* vol. 4, p. 679 – 688, 1944.

[25] J. P. Decker, "Some effects of temperature and carbon dioxide concentration on photosynthesis of Mimulus," in *Carnegie institution of Washington* , Stanford, California, June 1958.

[26] T. Yagishita, S. Sawayama, K. Tsukahara and T. Ogi, "Effects of glucose addition and light on current outputs in photosynthetic electrochemical cells using synechocystis sp. PCC6714," *J. bioscience and bioengineering,* vol. 88, no. 2, pp. 210-214, 1999.

[27] J. K. Paul and J. P. Decker, "Relation between light intensity and rate of photosynthesis of loblolly pine and certain hardwoods," *Plant physiology,* vol. 19, p. 350 – 358, 1944.

[28] M. A. Masadeh, K. Kuruvinashetti, M. Shahparnia, P. Pillay and M. Packirisamy, "Electrochemical Modeling and Equivalent Circuit Representation of a Microphotosynthetic Power Cell," *IEEE Trans. Ind. Electron,* vol. 64, no. 2, Feb. 2017, pp. 1561 - 1571, 2017.

[29] Z. Silvio, C. W. Robert, H.-C. I. Herbert and J. B. Lawrence, "Current Sensing Techniques: A Review," *IEEE SENSORS JOURNAL,* vol. 9, no. 4, p. 23, 2009.

[30] T. Min, H. Xiaozong and F. Dongbing, "A Simple Low Power Current Sensor Without Using Amplifier," in *2010 3rd International Conference on Computer Science and Information Technology*, Chengdu, China, 2010.

[31] M. N. Stan, L. Varzaru, V. Anghel and G. Brezeanu, "Winning the battle for low gain error and high CMRR — A current sense amplifier with trimmable gain resistors," in *International Semiconductor Conference (CAS)*, Sinaia, Romania, 2016.

[32] M. Taherzadeh-Sani, S. M. H. Hussaini, H. Rezaee-Dehsorkh, F. Nabki and M. Sawan, "A 170-dB Ω CMOS TIA With 52-pA Input-Referred Noise and 1-MHz Bandwidth for Very Low Current Sensing," *IEEE Transactions on Very Large Scale Integration (VLSI) Systems*, vol. 25, no. 5, May 2017, pp. 1756 - 1766, 2017.

[33] G. Hui, L. Jianmin and S. Beibei, "Design and application of an ultra low current digitizer with large dynamic range," in *Nuclear Science Symposium and Medical Imaging Conference (NSS/MIC), 2013 IEEE*, Seoul, South Korea, 2013.

[34] Texas Instruments, "OPAx277 High Precision Operational Amplifiers," OPA277P datasheet, March 1999 [Revised June, 2015].

[35] B. Logan, Microbial Fuel Cells. Hoboken, NJ, USA: Wiley, 2008.

[36] A. Gunawardena, "Performance of a Yeast-mediated Biological Fuel Cell," *Int. J. of Molecular Sci.*, vol. 9, no. 10, pp. 1893-1907, 2008.

[37] P. -W. Li, L. Schaefer and M. K. C hyu, "Multiple Transport Processes In Solid Oxide Fuel Cells," *WIT Trans. on State-of-the-art in Sci. and Eng.*, vol. 10, p. 41, 2005.

[38] B. Sundén, "Transport Phenomena in Fuel Cells," *WIT press*, vol. 19, p. 384 , 2005.

[39] S. Keith and H. Y. Eileen, Microbial Electrochemical and Fuel Cells: Fundamentals and Applications, Cambridge,UK: Woodhead Publishing, Nov. 2015.

[40] I. EG&G Technical Services, Fuel cell handbook (Seventh Edition), Morgantown, West Virginia: Parsons, Inc. for the National Energy Technology Laboratory,, 2004.

[41] Texas Instruments, "bq25504 Ultra Low-Power Boost Converter With Battery Management for Energy," bq25504 datasheet, Oct, 2011 [Revised June, 2015].

[42] E. Dallago, A. L. Barnabei, A. Liberale, G. Torelli and G. Venchi, "A 300-mV Low-Power Management System for Energy Harvesting Applications," *IEEE Trans. Power Electron.*, vol. 31, no. 3, pp. 2273 - 2281, 2016.

[43] A. V. Ramanan, "Energy Harvesting And Modeling Of Photosynthetic Power Cell," M.A.Sc. thesis, Dept., ECE, Concordia Univ., Canada,QC, 2013.